NASA TECHNICAL MEMORANDUM

NASA TM X-73332

THE SKYLAB ATM/S-056 X-RAY EVENT ANALYZER: INSTRUMENT DESCRIPTION, PARAMETER DETERMINATION, AND ANALYSIS EXAMPLE (15 JUNE 1973 1B/M3 FLARE)

By Robert M. Wilson
Space Sciences Laboratory

(NASA-TM-X-73332) SKYLAB ATM/S-056 X-RAY EVENT ANALYZER: INSTRUMENT DESCRIPTION, PARAMETER DETERMINATION, AND ANALYSIS EXAMPLE (15 JUNE 1973 1B/M3 FLARE) (NASA) 45 p HC $4.00 CSCL 14B G3/19

N76-32238

Unclas 02444

August 1976

NASA

George C. Marshall Space Flight Center
Marshall Space Flight Center, Alabama

TECHNICAL REPORT STANDARD TITLE PAGE

1. REPORT NO.	2. GOVERNMENT ACCESSION NO.	3. RECIPIENT'S CATALOG NO.
NASA TM X-73332		

4. TITLE AND SUBTITLE	5. REPORT DATE
The Skylab ATM/S-056 X-Ray Event Analyzer: Instrument Description, Parameter Determination, and Analysis Example (15 June 1973 1B/M3 Flare)	August 1976
	6. PERFORMING ORGANIZATION CODE
7. AUTHOR(S)	8. PERFORMING ORGANIZATION REPORT #
Robert M. Wilson	
9. PERFORMING ORGANIZATION NAME AND ADDRESS	10. WORK UNIT NO.
George C. Marshall Space Flight Center Marshall Space Flight Center, Alabama 35812	11. CONTRACT OR GRANT NO.
	13. TYPE OF REPORT & PERIOD COVERED
12. SPONSORING AGENCY NAME AND ADDRESS	
National Aeronautics and Space Administration Washington, D.C. 20546	Technical Memorandum
	14. SPONSORING AGENCY CODE

15. SUPPLEMENTARY NOTES

Prepared by Space Sciences Laboratory, Science and Engineering

16. ABSTRACT

The Skylab ATM/S-056 X-Ray Event Analyzer, part of the NASA-Marshall Space Flight Center/The Aerospace Corporation x-ray telescope experiment, is described. The techniques employed in the analysis of its data to determine electron temperatures and emission measures are reviewed. The analysis of a sample event — the 15 June 1973 1B/M3 flare — is performed. Comparison of the X-Ray Event Analyzer data with that of the SOLRAD 9 observations indicates that the X-Ray Event Analyzer accurately monitored the Sun's 2.5 to 7.25 Å x-ray emission and to a lesser extent the 6.1 to 20 Å emission. A mean average peak temperature of 15×10^6 K at 1412 UT and a mean average peak electron density (assuming a flare volume of 10^{28} cm^3) of 2.7×10^{10} cm^{-3} at 1416 to 1417 UT are deduced for the event. The X-Ray Event Analyzer data, having a 2.5 s time resolution, should be invaluable in comparisons with other high-time resolution data (e.g., radio bursts).

17. KEY WORDS	18. DISTRIBUTION STATEMENT
	Robert M Wilson Unclassified — Unlimited

19. SECURITY CLASSIF. (of this report)	20. SECURITY CLASSIF. (of this page)	21. NO. OF PAGES	22. PRICE
Unclassified	Unclassified	45	NTIS

ACKNOWLEDGMENTS

Appreciation is expressed to Dr. D. L. McKenzie of The Aerospace Corporation for providing the original model spectrum-versus-temperature tables and for helpful discussions concerning proportional counters in general. Also, the author is indebted to Dr. W. Henze (Teledyne-Brown Engineering Co.), Mr. J. Smith (NOAA/Space Environment Laboratory), Dr. K. Krall (University of Alabama in Huntsville), and Mr. E. Reichmann (NASA/Marshall Space Flight Center) who have studied in detail the S-056 x-ray images, H-alpha filtergrams, and KPNO magnetograms, and who have provided enlightenment concerning the intricacies of this complex event. Appreciation is expressed to Dr. D. Horan (Naval Research Laboratory) for providing the SOLRAD 9 data, to Dr. C. Cheng (Ball Brothers Research Corporation) for helpful discussions concerning the temperature profile of the event, to Mr. O. Weaver for tabulating the raw and converted data, and to Drs. E. Tandberg-Hanssen (S-056/MSFC, PI) and A. C. deLoach (S-056/MSFC CoI) for critically reviewing the manuscript. This work was performed, in part, to serve as a contribution to the Skylab Solar Workshop Series B on Solar Flares.

TABLE OF CONTENTS

LIST OF ILLUSTRATIONS

LIST OF ILLUSTRATIONS (Concluded)

LIST OF TABLES

TECHNICAL MEMORANDUM X-73332

THE SKYLAB ATM/S-056 X-RAY EVENT ANALYZER: INSTRUMENT DESCRIPTION, PARAMETER DETERMINATION, AND ANALYSIS EXAMPLE (15 JUNE 1973 1B/M3 FLARE)

I. INTRODUCTION

Gas-filled x-ray detectors have been utilized extensively in solar and cosmic x-ray astronomy. These detectors include the ionization chamber, the Geiger-Müller tube, and the proportional counter, all sharing one common characteristic, i.e., their principle of operation is the absorption of x-rays. Hoover et al. [1] have described the basic theory of x-ray detectors and discussed how they are used in solar and cosmic x-ray astronomy investigations.

A proportional counter, so called because the mean amplitude of its output pulse is proportional to the energy of the incident x-ray photon, is typically a small cylindrical volume containing a central wire (anode) held at a high positive potential with respect to its outer wall (cathode). Electrons generated in the gas from the primary ionizing x-ray photon are accelerated toward the anode and acquire enough energy to produce further ion-electron pairs by collisions with the neutral gas atoms, thus causing a cascade or avalanche of electrons which drift toward the anode where they are collected. The avalanche contains M electrons for each ion pair generated in the ionizing event and an associated M positive ions which move toward the cathode, thus producing a pulse of current in the external measuring circuits. The parameter M is known as the "gas multiplication factor," or more simply the "gas gain," of the counter and has a Gaussian distribution about a mean value proportional to the incident x-ray energy. Thus, by analyzing the distribution of pulse amplitudes from a proportional counter, one obtains information regarding the spectrum of the incident x-ray flux. In general, multichannel pulse-height analyzers, which separate or discriminate pulses into several selective amplitude ranges, are used to investigate the pulse amplitude distribution and extract the spectral data.

Gas-filled x-ray detectors, in particular proportional counters utilizing multichannel pulse-height analyzers, in addition to their ability to detect and monitor solar activity with high time resolution (e.g., the occurrence of x-ray enhancements associated with H-alpha flares or eruptive prominence events or radio bursts) can also be used to probe the physical conditions of the solar plasma volume, i.e., the electron temperature and emission measure. Horan [2] and Dere et al. [3] have discussed the determination of these quantities using ionization chamber data, a technique which can also be applied to proportional counter data and which is similar to techniques employed by Vaiana et al. [4], Walker et al. [5], Vorpahl et al. [6], and Smith et al. [7,8] in the determination of linear physical parameters from x-ray photographic data.

The purpose of this report is to describe the Skylab ATM/S-056 X-Ray Event Analyzer (part of the NASA-Marshall Space Flight Center/The Aerospace Corporation x-ray telescope experiment), an x-ray proportional counter system employing multichannel pulse-height analyzers; to describe the methods used in the analysis of its data; and to report results of analysis for a selected event — the 15 June 1973 1B/M3 flare.

II. INSTRUMENT DESCRIPTION

The Skylab ATM/S-056 experiment consisted of two scientific instruments: the X-Ray Telescope, which recorded solar x-ray emission on photographic film through several x-ray filters with high spatial and temporal resolution, and the X-Ray Event Analyzer (X-REA), which recorded solar x-ray emission by means of a proportional counter system employing multichannel pulse-height analyzers. The overall experiment design, stressing primarily the X-Ray Telescope, has been described by Walsh et al. [9] and Underwood et al. [10]; deLoach et al. [11] have summarized the orbital and ground-testing performance of the instruments.

The X-REA consisted of two conventional, coaxial proportional counters mounted inside a single housing. The two counters were designated the "beryllium counter" and the "aluminum counter" because of their window material. The beryllium counter had a window thickness of 2.54×10^{-2} cm and was 1.27 cm in diameter. Further, it had a gas mix of xenon-methane (90-10 percent) at 1 atm and responded to the 2.5 to 7.25 Å x-ray flux, separating the pulses into 6 wavelength ranges (channels). The aluminum counter had a window thickness of 6.35×10^{-4} cm and was 3.18×10^{-1} cm in diameter. The

window was supported by an aluminum mesh with an estimated transmission of 80 percent. Further, the counter had a gas mix of argon-methane (90-10 percent) at 1 atm and responded to the 6.1 to 20 Å x-ray flux, separating the pulses into 4 wavelength ranges (channels). Both counters were 2.22 cm in length and contained a central tungsten wire anode 5.08×10^{-3} cm in thickness.

Because both counters were essentially uncollimated, both viewed the full Sun and thus had no spatial resolution. Events observed in the counters, however, could clearly be associated with particular events occurring on the Sun as long as two or more events did not occur simultaneously. The correlation of X-REA events and solar activity phenomena was achieved via a comparison of the X-REA telemetry records with information contained in Solar-Geophysical Data and with photographic images observed by the X-Ray Telescope.

The pulses in each output channel were accumulated for 2.5 s, and the accumulated total was transferred to an output buffer register which automatically erased previous data in the buffer. The 10 ripple-through counters in the digital signal conditioner were read sequentially, once every 250 ms, and telemetry sampled the buffer four times per second.

Since the maximum count rate of the tubes was approximately 6×10^3 counts s^{-1}, a four-position aperture wheel (6.35 cm diameter) was fitted in front of each counter window to increase the dynamic range of the X-REA. Successive apertures varied by approximately four times in area; thus, the smallest aperture (aperture 1) was approximately 64 times smaller in area than the largest aperture (aperture 4). The apertures could be changed by stepper motors manually by the astronaut at the Apollo Telescope Mount (ATM) control and display panel or, more often, automatically by the electronics which switched apertures when the counting rate reached a certain prescribed level.

An inflight functional check of the electronics was provided by internal calibrators, one for each proportional counter subsystem. Each calibrator consisted of a unijunction oscillator followed by a divider circuit. The calibration signals were terminated when the high voltage power supplies for the counters were turned on. No onboard calibration sources were provided.

In addition to the telemetered counts, the total count rate from all channels in each subsystem was monitored and displayed on the ATM control and display panel. The counter rate as a function of time was also displayed

on a plotter (i.e., the history plotter) mounted on the ATM control and display panel. These devices provided the astronaut a real-time indication of solar x-ray activity and a record of activity versus time, thereby enabling him to select the best mode of operation for the X-Ray Telescope.

Figure 1 schematically describes the functional aspects of an X-REA proportional counter subsystem, while Tables 1 and 2 summarize the X-REA physical weight, dimensions, etc., and channel characteristics, respectively. For additional comments concerning the X-REA, see Reference [12].

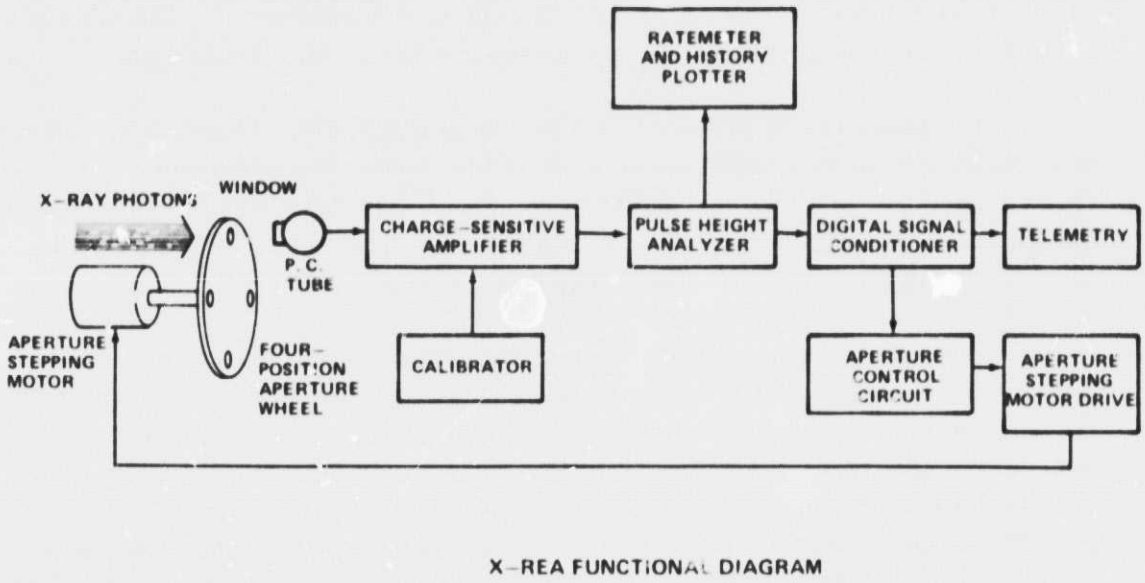

Figure 1. Functional diagram of typical X-REA proportional counter subsystem.

TABLE 1. X-REA EXPERIMENT PARAMETERS

System Parameters:

Weight — ~17 kg
Size — ~0.142 × 0.157 × 0.183 m
Power (Avg) — ~15 W at 28 Vdc
Temperature Limits — 0 to 40°C
(Allowable Operating)

TABLE 1. (Concluded)

Data Storage — ATM I&C Tape Recorder
Data Rate — 20 Bits/2.5 s
High Voltage — 1600 to 2300 Vdc (Tuneable)
Field of View — few degrees
Temporal Resolution — 2.5 s

Aluminum Counter:

Wavelength Range — 6.1 to 20 Å
Pulse Height Analyzer Channels — 4
Spectral Resolution — ~4 Å
Window (Thickness) — 6.35×10^{-4} cm Aluminum (1.71 mg cm^{-2}) on Aluminum Mesh (80 percent transparent)
Gas Mix — Argon-Methane (90-10 percent)
Aperture Areas — 1 2.45×10^{-3} cm^2
2 5.35×10^{-3} cm^2
3 2.04×10^{-2} cm^2
4[a] 7.92×10^{-2} cm^2

Beryllium Counter:

Wavelength Range — 2.5 to 7.25 Å
Pulse Height Analyzer Channels — 6
Spectral Resolution — ~0.5 Å
Window (Thickness) — 2.54×10^{-2} cm^2 Beryllium (46.2 mg cm^{-2})
Gas Mix — Xenon-Methane (90-10 percent)
Aperture Areas — 1 2.04×10^{-2} cm^2
2 8.11×10^{-2} cm^2
3 3.22×10^{-1} cm^2
4[a] 1.27 cm^2

a. Corresponds to area of tube window.

TABLE 2. X-REA CHANNEL CHARACTERISTICS

Aluminum Counter			
Channel	Wavelength Range	$\bar{\eta}(\bar{\lambda})$[a]	$\bar{\lambda}(\bar{\epsilon})$[b]
1	16 to 20 Å	0.0056	18 Å (1.10×10^{-9})
2	12 to 16 Å	0.071	14 Å (1.41×10^{-9})
3	8 to 12 Å	0.007	10 Å (1.98×10^{-9})
4	6.1 to 8 Å	0.35	7.05 Å (2.81×10^{-9})
Total	6.1 to 20 Å	0.1084	13.05 Å (1.52×10^{-9})
Beryllium Counter			
Channel	Wavelength Range	$\bar{\eta}(\bar{\lambda})$[c]	$\bar{\lambda}(\bar{\epsilon})$[b]
1	6 to 7.25 Å	0.077	6.63 Å (2.99×10^{-9})
2	5.5 to 6 Å	0.157	5.75 Å (3.44×10^{-9})
3	5 to 5.5 Å	0.20	5.25 Å (3.77×10^{-9})
4	4.5 to 5 Å	0.23	4.75 Å (4.17×10^{-9})
5	3.75 to 4.5 Å	0.42	4.13 Å (4.79×10^{-9})
6	2.5 to 3.75 Å	0.66	3.13 Å (6.33×10^{-9})
Total	2.5 to 7.25 Å	0.29	4.88 Å (4.06×10^{-9})

a. Excludes aluminum mesh transmittance (assumed to be 80 percent).
b. $\bar{\lambda}$ is mean wavelength; $\bar{\epsilon}$ is mean photon energy, calculated by the equation $\bar{\epsilon} = 1.98 \times 10^{-8}$ erg · Å/$\bar{\lambda}$ (Å).
c. $\bar{\eta}$ is mean counter efficiency per interval mean wavelength ($\bar{\lambda}$).

III. PHYSICAL PARAMETER DETERMINATION

All of the solar soft x-radiation which reaches the Earth originates in the corona. This x-ray energy is mostly generated by resonance-line emission from highly ionized atomic species and by free-free and free-bound continuum processes, although various forbidden line emissions, as well as the two-photon continua, also contribute. Walker [13, 14] has made an in-depth review of the coronal x-ray spectrum, and Doschek [15, 16] has reviewed the spectrum of the flaring Sun. Also, Kahler [17] has examined the thermal and nonthermal interpretations of flare x-ray bursts [18, 19], and DeJager et al. [20] have summarized some recent observational data on solar flares.

Previous spectral measurements indicated that the temperature during flares exceeds 10×10^6 K, and occasionally probably exceeds 30×10^6 K [21, 22]. The Aerospace Corporation has developed a comprehensive program for the computation of the thermal x-ray spectra.[1] This program has been applied to the X-REA by folding the theoretical spectra through the calculated response of the X-REA counters. The resulting model spectrum for each counter appears in Tables 3 and 4. The units of the individual entries are counts per second per square centimeter per unit emission measure of the emitting object on the Sun. Ratios between channels in any one counter or ratios between sums of channels of both counters are therefore equivalent to similar ratios of the model X-REA spectrum. Thus, a determination of the plasma electron temperature is possible. Table 5 gives several selected ratios for the temperature regime of 2 to 30×10^6 K which have been used in temperature determination studies.

A determination of the emission measure[2] is straightforward once the temperature is known. It can be shown that if ϕ_j is the output counts $cm^{-2}\ s^{-1}$ from the X-REA for a particular channel j and F_j is the calculated X-REA response for the same channel deduced from Table 3 or 4, then the emission measure, denoted EM, can be written as

1. Private communication with D. L. McKenzie.

2. Private communication with W. Henze.

TABLE 3. X-REA ALUMINUM COUNTER MODEL SPECTRUM VERSUS TEMPERATURE (UNITS ARE COUNTS cm^{-2} s^{-1} EM^{-1})

Temperature (K)	1	2	3	4	Total
2.0×10^6	1.63 (-45)	4.28 (-45)	3.37 (-45)	3.92 (-46)	9.67 (-45)
2.5×10^6	3.20 (-45)	9.50 (-45)	1.13 (-44)	1.28 (-45)	2.53 (-44)
3.0×10^6	4.01 (-45)	1.38 (-44)	2.01 (-44)	2.57 (-45)	4.05 (-44)
3.5×10^6	4.22 (-45)	1.64 (-44)	2.97 (-44)	4.15 (-45)	5.45 (-44)
4.0×10^6	4.22 (-45)	1.82 (-44)	4.01 (-44)	5.98 (-45)	6.85 (-44)
4.5×10^6	3.91 (-45)	1.83 (-44)	4.75 (-44)	7.53 (-45)	7.72 (-44)
5.0×10^6	3.67 (-45)	1.83 (-44)	5.53 (-44)	9.38 (-45)	8.67 (-44)
5.5×10^6	3.38 (-45)	1.75 (-44)	5.88 (-44)	1.06 (-44)	9.03 (-44)
6.0×10^6	3.21 (-45)	1.71 (-44)	6.18 (-44)	1.19 (-44)	9.40 (-44)
6.5×10^6	3.09 (-45)	1.68 (-44)	6.36 (-44)	1.30 (-44)	9.65 (-44)
7.0×10^6	3.01 (-45)	1.65 (-44)	6.46 (-44)	1.40 (-44)	9.81 (-44)
7.5×10^6	2.97 (-45)	1.63 (-44)	6.35 (-44)	1.46 (-44)	9.74 (-44)
8.0×10^6	2.94 (-45)	1.62 (-44)	6.37 (-44)	1.51 (-44)	9.79 (-44)
8.5×10^6	2.94 (-45)	1.61 (-44)	6.23 (-44)	1.54 (-44)	9.67 (-44)
9.0×10^6	2.94 (-45)	1.61 (-44)	6.13 (-44)	1.55 (-44)	9.58 (-44)

TABLE 3. (Concluded)

Temperature (K)	1	2	3	4	Total
9.5×10^6	2.96 (-45)	1.62 (-44)	6.08 (-44)	1.57 (-44)	9.57 (-44)
10.0×10^6	2.98 (-45)	1.63 (-44)	6.02 (-44)	1.57 (-44)	9.52 (-44)
11.0×10^6	3.00 (-45)	1.65 (-44)	5.93 (-44)	1.57 (-44)	9.45 (-44)
12.0×10^6	3.01 (-45)	1.66 (-44)	5.95 (-44)	1.59 (-44)	9.50 (-44)
13.0×10^6	3.05 (-45)	1.69 (-44)	6.01 (-44)	1.61 (-44)	9.62 (-44)
14.0×10^6	3.08 (-45)	1.71 (-44)	6.06 (-44)	1.64 (-44)	9.72 (-44)
15.0×10^6	3.10 (-45)	1.73 (-44)	6.12 (-44)	1.65 (-44)	9.81 (-44)
16.0×10^6	3.13 (-45)	1.75 (-44)	6.21 (-44)	1.68 (-44)	9.95 (-44)
17.0×10^6	3.13 (-45)	1.76 (-44)	6.24 (-44)	1.68 (-44)	9.99 (-44)
18.0×10^6	3.14 (-45)	1.77 (-44)	6.28 (-44)	1.69 (-44)	1.01 (-43)
19.0×10^6	3.16 (-45)	1.78 (-44)	6.35 (-44)	1.71 (-44)	1.02 (-43)
20.0×10^6	3.18 (-45)	1.80 (-44)	6.42 (-44)	1.73 (-44)	1.03 (-43)
22.0×10^6	3.19 (-45)	1.81 (-44)	6.54 (-44)	1.77 (-44)	1.04 (-43)
24.0×10^6	3.20 (-45)	1.83 (-44)	6.62 (-44)	1.80 (-44)	1.06 (-43)
26.0×10^6	3.20 (-45)	1.84 (-44)	6.69 (-44)	1.82 (-44)	1.07 (-43)
28.0×10^6	3.19 (-45)	1.84 (-44)	6.73 (-44)	1.83 (-44)	1.07 (-43)
30.0×10^6	3.19 (-45)	1.84 (-44)	6.76 (-44)	1.85 (-44)	1.08 (-43)

TABLE 4. X-REA BERYLLIUM COUNTER MODEL SPECTRUM VERSUS TEMPERATURE (UNITS ARE COUNTS cm^{-2} s^{-1} EM^{-1})

Temperature (K)	1	2	3	4	5	6	Total
2.0×10^6	3.35 (-48)	1.14 (-48)	7.83 (-49)	4.17 (-49)	1.99 (-49)	2.09 (-50)	5.91 (-48)
2.5×10^6	2.02 (-47)	8.19 (-48)	7.09 (-48)	4.98 (-48)	3.03 (-48)	4.84 (-49)	4.40 (-47)
3.0×10^6	5.78 (-47)	2.72 (-47)	2.76 (-47)	2.27 (-47)	1.94 (-47)	4.10 (-48)	1.59 (-46)
3.5×10^6	1.26 (-46)	6.53 (-47)	7.37 (-47)	6.71 (-47)	5.86 (-47)	1.86 (-47)	4.09 (-46)
4.0×10^6	2.27 (-46)	1.26 (-46)	1.52 (-46)	1.48 (-46)	1.46 (-46)	5.67 (-47)	8.56 (-46)
4.5×10^6	3.40 (-46)	1.97 (-46)	2.47 (-46)	2.51 (-46)	2.76 (-46)	1.25 (-46)	1.44 (-45)
5.0×10^6	4.91 (-46)	2.94 (-46)	3.82 (-46)	4.02 (-46)	4.75 (-46)	2.46 (-46)	2.29 (-45)
5.5×10^6	6.46 (-46)	3.99 (-46)	5.29 (-46)	5.75 (-46)	7.25 (-46)	4.22 (-46)	3.30 (-45)
6.0×10^6	8.19 (-46)	5.22 (-46)	7.10 (-46)	7.87 (-46)	1.03 (-45)	6.66 (-46)	4.53 (-45)
6.5×10^6	1.01 (-45)	6.52 (-46)	9.06 (-46)	1.02 (-45)	1.39 (-45)	9.92 (-46)	5.97 (-45)
7.0×10^6	1.18 (-45)	7.87 (-46)	1.12 (-45)	1.29 (-45)	1.81 (-45)	1.40 (-45)	7.64 (-45)
7.5×10^6	1.35 (-45)	9.29 (-46)	1.33 (-45)	1.56 (-45)	2.28 (-45)	1.91 (-45)	9.36 (-45)
8.0×10^6	1.54 (-45)	1.08 (-45)	1.57 (-45)	1.87 (-45)	2.77 (-45)	2.47 (-45)	1.13 (-44)
8.5×10^6	1.65 (-45)	1.20 (-45)	1.78 (-45)	2.15 (-45)	3.28 (-45)	3.12 (-45)	1.32 (-44)
9.0×10^6	1.79 (-45)	1.34 (-45)	2.02 (-45)	2.47 (-45)	3.85 (-45)	3.83 (-45)	1.53 (-44)
9.5×10^6	1.91 (-45)	1.46 (-45)	2.24 (-45)	2.80 (-45)	4.46 (-45)	4.68 (-45)	1.76 (-44)

TABLE 4. (Concluded)

Temperature (K)	1	2	3	4	5	6	Total
10.0×10^6	2.06 (-45)	1.62 (-45)	2.50 (-45)	3.15 (-45)	5.12 (-45)	5.59 (-45)	2.00 (-44)
11.0×10^6	2.24 (-45)	1.86 (-45)	2.95 (-45)	3.80 (-45)	6.35 (-45)	7.46 (-45)	2.47 (-44)
12.0×10^6	2.36 (-45)	2.06 (-45)	3.34 (-45)	4.40 (-45)	7.62 (-45)	9.61 (-45)	2.94 (-44)
13.0×10^6	2.48 (-45)	2.23 (-45)	3.69 (-45)	4.95 (-45)	8.90 (-45)	1.18 (-44)	3.41 (-44)
14.0×10^6	2.56 (-45)	2.38 (-45)	4.01 (-45)	5.46 (-45)	9.92 (-45)	1.40 (-44)	3.83 (-44)
15.0×10^6	2.61 (-45)	2.48 (-45)	4.24 (-45)	5.88 (-45)	1.10 (-44)	1.67 (-44)	4.29 (-44)
16.0×10^6	2.69 (-45)	2.61 (-45)	4.52 (-45)	6.35 (-45)	1.21 (-44)	1.87 (-44)	4.70 (-44)
17.0×10^6	2.68 (-45)	2.63 (-45)	4.59 (-45)	6.57 (-45)	1.29 (-44)	2.09 (-44)	5.03 (-44)
18.0×10^6	2.69 (-45)	2.66 (-45)	4.67 (-45)	6.76 (-45)	1.35 (-44)	2.31 (-44)	5.34 (-44)
19.0×10^6	2.72 (-45)	2.70 (-45)	4.77 (-45)	7.01 (-45)	1.43 (-44)	2.54 (-44)	5.69 (-44)
20.0×10^6	2.76 (-45)	2.76 (-45)	4.89 (-45)	7.25 (-45)	1.51 (-44)	2.75 (-44)	6.03 (-44)
22.0×10^6	2.83 (-45)	2.83 (-45)	5.07 (-45)	7.62 (-45)	1.63 (-44)	3.16 (-44)	6.63 (-44)
24.0×10^6	2.87 (-45)	2.88 (-45)	5.17 (-45)	7.87 (-45)	1.72 (-44)	3.54 (-44)	7.14 (-44)
26.0×10^6	2.92 (-45)	2.94 (-45)	5.29 (-45)	8.11 (-45)	1.82 (-44)	3.91 (-44)	7.66 (-44)
28.0×10^6	2.95 (-45)	2.96 (-45)	5.35 (-45)	8.35 (-45)	1.89 (-44)	4.24 (-44)	8.09 (-44)
30.0×10^6	2.98 (-45)	3.01 (-45)	5.45 (-45)	8.50 (-45)	1.95 (-44)	4.55 (-44)	8.49 (-44)

TABLE 5. SELECTED MODEL SPECTRUM RATIOS VERSUS TEMPERATURE

Temperature (K)	Be $\frac{6}{5}$	Al $\frac{4}{3}$	$\frac{\text{Be } 5+6}{\text{Al } 3+4}$	$\frac{\text{Be T}}{\text{Al T}}$	$\frac{\text{Be } 5+6}{\text{Be T}}$	$\frac{\text{Be } 5+6}{\text{Al T}}$
2.0×10^6	1.05 (-1)	1.16 (-1)	5.85 (-5)	6.11 (-4)	3.72 (-2)	2.27 (-5)
2.5×10^6	1.60 (-1)	1.13 (-1)	2.79 (-4)	1.74 (-3)	7.99 (-2)	1.39 (-4)
3.0×10^6	2.11 (-1)	1.28 (-1)	1.04 (-3)	3.93 (-3)	1.48 (-1)	5.80 (-4)
3.5×10^6	3.17 (-1)	1.40 (-1)	2.28 (-3)	7.50 (-3)	1.89 (-1)	1.42 (-3)
4.0×10^6	3.88 (-1)	1.49 (-1)	4.40 (-3)	1.25 (-2)	2.37 (-1)	2.96 (-3)
4.5×10^6	4.53 (-1)	1.59 (-1)	7.29 (-3)	1.87 (-2)	2.78 (-1)	5.19 (-3)
5.0×10^6	5.18 (-1)	1.70 (-1)	1.11 (-2)	2.64 (-2)	3.15 (-1)	8.32 (-3)
5.5×10^6	5.82 (-1)	1.80 (-1)	1.44 (-2)	3.65 (-2)	3.48 (-1)	1.27 (-2)
6.0×10^6	6.47 (-1)	1.93 (-1)	2.31 (-2)	4.82 (-2)	3.74 (-1)	1.80 (-2)
6.5×10^6	7.14 (-1)	2.04 (-1)	3.11 (-2)	6.19 (-2)	3.99 (-1)	2.47 (-2)
7.0×10^6	7.73 (-1)	2.17 (-1)	4.08 (-2)	7.79 (-2)	4.20 (-1)	3.27 (-2)
7.5×10^6	8.38 (-1)	2.30 (-1)	5.36 (-2)	9.61 (-2)	4.48 (-1)	4.30 (-2)
8.0×10^6	8.92 (-1)	2.37 (-1)	6.65 (-2)	1.15 (-1)	4.64 (-1)	5.35 (-2)
8.5×10^6	9.51 (-1)	2.47 (-1)	8.24 (-2)	1.37 (-1)	4.85 (-1)	6.62 (-2)
9.0×10^6	9.95 (-1)	2.53 (-1)	1.00 (-1)	1.60 (-1)	5.02 (-1)	8.02 (-2)
9.5×10^6	1.05 (0)	2.58 (-1)	1.19 (-1)	1.84 (-1)	5.19 (-1)	9.55 (-2)

TABLE 5. (Concluded)

Temperature (K)	Be $\frac{6}{5}$	Al $\frac{4}{3}$	$\frac{\text{Be } 5+6}{\text{Al } 3+4}$	$\frac{\text{Be T}}{\text{Al T}}$	$\frac{\text{Be } 5+6}{\text{Be T}}$	$\frac{\text{Be } 5+6}{\text{Al T}}$
10.0×10^6	1.09 (0)	2.61 (-1)	1.41 (-1)	2.10 (-1)	5.36 (-1)	1.13 (-1)
11.0×10^6	1.17 (0)	2.65 (-1)	1.84 (-1)	2.61 (-1)	5.59 (-1)	1.46 (-1)
12.0×10^6	1.26 (0)	2.67 (-1)	2.28 (-1)	3.09 (-1)	5.86 (-1)	1.81 (-1)
13.0×10^6	1.33 (0)	2.68 (-1)	2.72 (-1)	3.54 (-1)	6.07 (-1)	2.15 (-1)
14.0×10^6	1.41 (0)	2.71 (-1)	3.10 (-1)	3.94 (-1)	6.25 (-1)	2.46 (-1)
15.0×10^6	1.52 (0)	2.70 (-1)	3.56 (-1)	4.37 (-1)	6.46 (-1)	2.82 (-1)
16.0×10^6	1.55 (0)	2.71 (-1)	3.90 (-1)	4.72 (-1)	6.55 (-1)	3.10 (-1)
17.0×10^6	1.62 (0)	2.69 (-1)	4.27 (-1)	5.04 (-1)	6.72 (-1)	3.38 (-1)
18.0×10^6	1.71 (0)	2.69 (-1)	4.59 (-1)	5.29 (-1)	6.85 (-1)	3.62 (-1)
19.0×10^6	1.78 (0)	2.69 (-1)	4.93 (-1)	5.58 (-1)	6.98 (-1)	3.89 (-1)
20.0×10^6	1.82 (0)	2.69 (-1)	5.23 (-1)	5.85 (-1)	7.06 (-1)	4.14 (-1)
22.0×10^6	1.94 (0)	2.71 (-1)	5.76 (-1)	6.38 (-1)	7.22 (-1)	4.61 (-1)
24.0×10^6	2.06 (0)	2.72 (-1)	6.25 (-1)	6.74 (-1)	7.37 (-1)	4.96 (-1)
26.0×10^6	2.15 (0)	2.72 (-1)	6.73 (-1)	7.16 (-1)	7.48 (-1)	5.36 (-1)
28.0×10^6	2.24 (0)	2.72 (-1)	7.16 (-1)	7.56 (-1)	7.58 (-1)	5.73 (-1)
30.0×10^6	2.33 (0)	2.74 (-1)	7.55 (-1)	7.86 (-1)	7.66 (-1)	6.02 (-1)

$$EM = \int N_e^2 \, dV = \frac{\psi_j}{F_j} \quad , \tag{1}$$

where N_e is the electron density and V is the volume of the emitting plasma. By assuming a volume, a determination of the electron density is accomplished; i.e.,

$$N_e = \left[\left(\frac{\psi_j}{F_j} \right) \left(\frac{1}{V} \right) \right]^{1/2} \quad . \tag{2}$$

IV. ANALYSIS EXAMPLE (15 JUNE 1973 1B/M3 FLARE)

The example chosen to illustrate the analysis using the X-REA data is the 15 June 1973 1B/M3, H-alpha two-ribbon flare which occurred in McMath 12379 (NOAA active region AR131) at N17W32 around 1413 UT (H-alpha Max) as reported by Hirman et al. [23]. This flare [24] was chosen because it was the major flare of the first manned Skylab mission and good correlation was possible between a number of Skylab and other instruments. Also, because it occurred in the first manned mission, the data should be very reliable, not suffering from the deterioration associated with methane-quenched counters (McKenzie, private communication).

The telemetered X-REA data (i.e., the "raw" data) have units of counts per aperture area per 2.5 s. Since it is desirable to have the output of both counters expressed in counts cm^{-2} s^{-1} and since the aperture areas are not equal for the same aperture number, the data must be adjusted accordingly. This is accomplished by correcting for aperture area and time, so that the units are now counts cm^{-2} s^{-1} (converted). These counts are designated "converted" because they still are not the true or "correct" count rates incident on the surface of the counter window. The correct counts are obtained by multiplying the converted values by the appropriate inverse of X-REA efficiency term and, when appropriate, adjusting for the degradation of the counter tubes, known to be a problem in the latter part of the Skylab mission. However, the

converted count rates are proportional to the true count rates, and because the theoretical response functions have taken into account the efficiencies of the counters, only converted count rates are used in plots of the data. Also, because the degradation of the tubes did not manifest itself until late in the Skylab mission, a knowledge of their degradation functions is not required for events occurring in the first and part of the second manned missions.

Figures 2 and 3 show the count rates for selected energy channels and the totals of the beryllium counter (Fig. 2) and the aluminum counter (Fig. 3). Figure 4 depicts the same event as observed by SOLRAD 9. A comparison of the X-REA data with the SOLRAD 9 data is accomplished by normalizing the data with respect to the peak of the event. This comparison is shown in Figures 5 and 6, where only the total beryllium (Fig. 5) and aluminum count (Fig. 6) rates are compared with the SOLRAD 9 1 to 8 Å and 8 to 20 Å fluxes, respectively. Since the SOLRAD 9 memory data have a time resolution of 1 min, the X-REA data have been averaged correspondingly.

Very close agreement is observed between the beryllium counter and the SOLRAD 9 1 to 8 Å data, both showing peak fluxes at 1414 UT. Similar rise and fall curves are noted during the period bounding the peak, i.e., 1406 to 1446 UT. Some discrepancy is noted prior to 1406 UT and may be attributed to noisy SOLRAD 9 1 to 8 Å data, since the background count levels were enhanced between 1346 to 1406 UT. It is concluded that the X-REA beryllium counter properly recorded the whole Sun x-ray emission and that observed variations in the X-REA data are real and represent actual variations in the intensity of the solar x-ray emission.

Concerning the comparison of the X-REA aluminum counter and the SOLRAD 9 8 to 20 Å data, similar peak occurrence times are found between 1415 and 1418 UT. However, the preflare, flare rise, and flare fall normalized flux curves are different. The preflare X-REA aluminum counter levels are somewhat higher than the SOLRAD 9 8 to 20 Å levels, by a factor of approximately 1.6. Also, the X-REA aluminum counter shows an emission decay rate of 0.29/min between 1420 and 1440 UT, which is to be compared to the rate of 0.34/min for the SOLRAD instrument. Knowledge of the SOLRAD 9 8 to 20 Å rise phase is incomplete because of data dropout between 1402 and 1408 UT; therefore, a good comparison of the two instruments during this phase cannot be accomplished. Between 1409 and 1415 UT, however, the two counters displayed similar rise curves, with the X-REA counter always showing slightly higher values. The aforementioned discrepancies may be attributed to noise

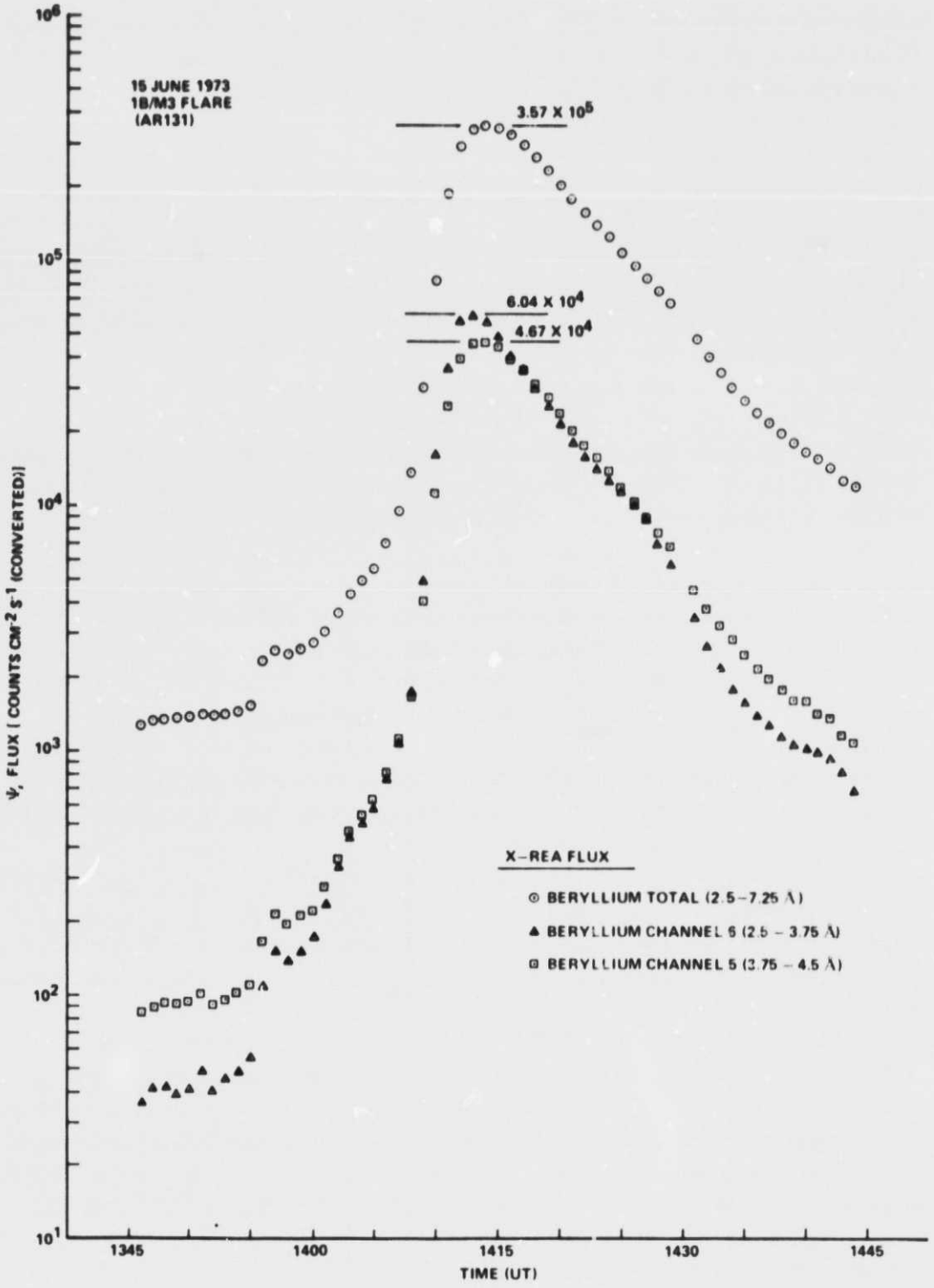

Figure 2. X-REA flux (beryllium counter total, channel 6 and channel 5) for the 15 June 1973 1B/ M3 flare in AR131 (1346 to 1444 UT).

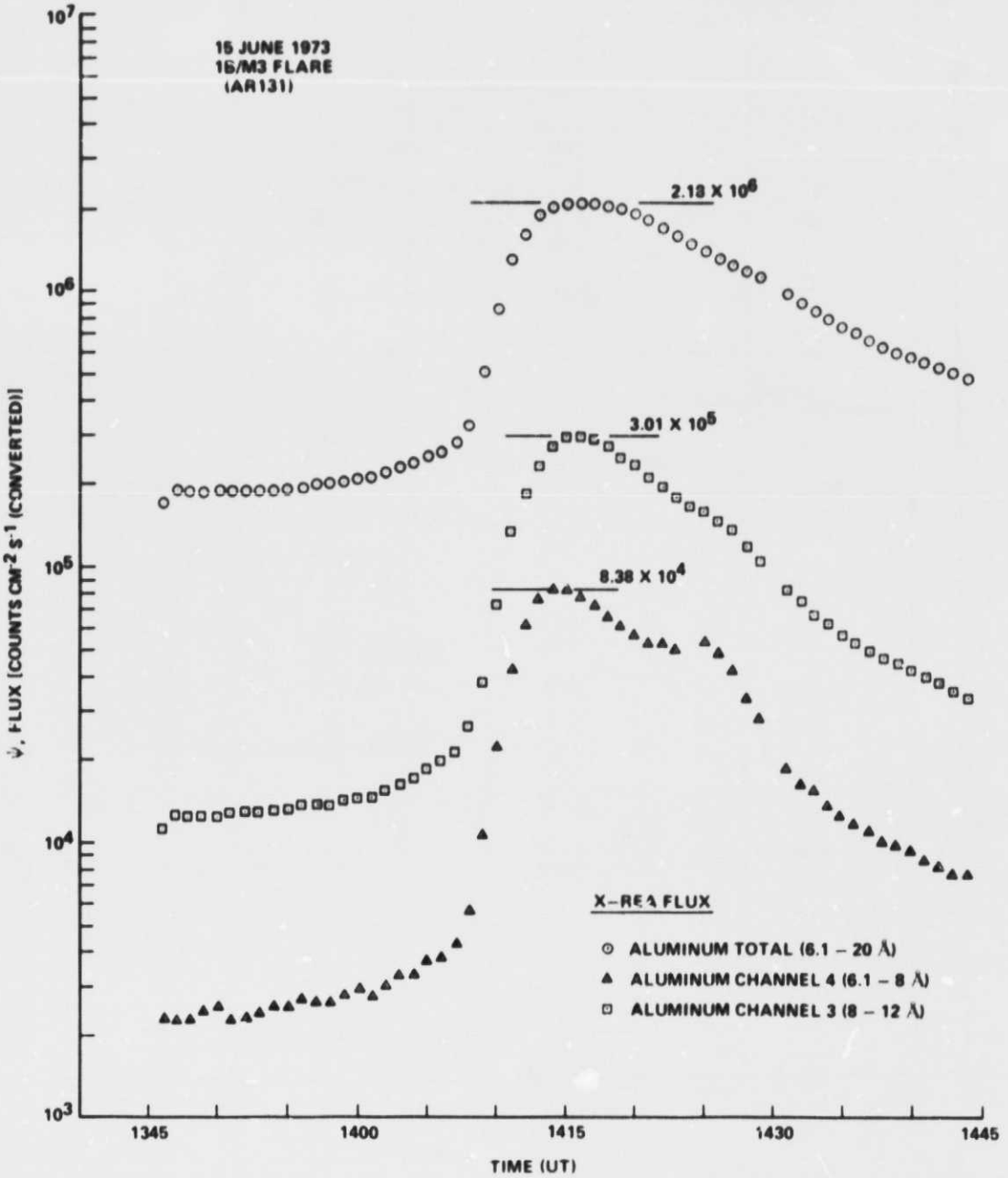

Figure 3. X-REA flux (aluminum counter total, channel 4 and channel 3) for the 15 June 1973 1B/ M3 flare in AR131 (1346 to 1444 UT).

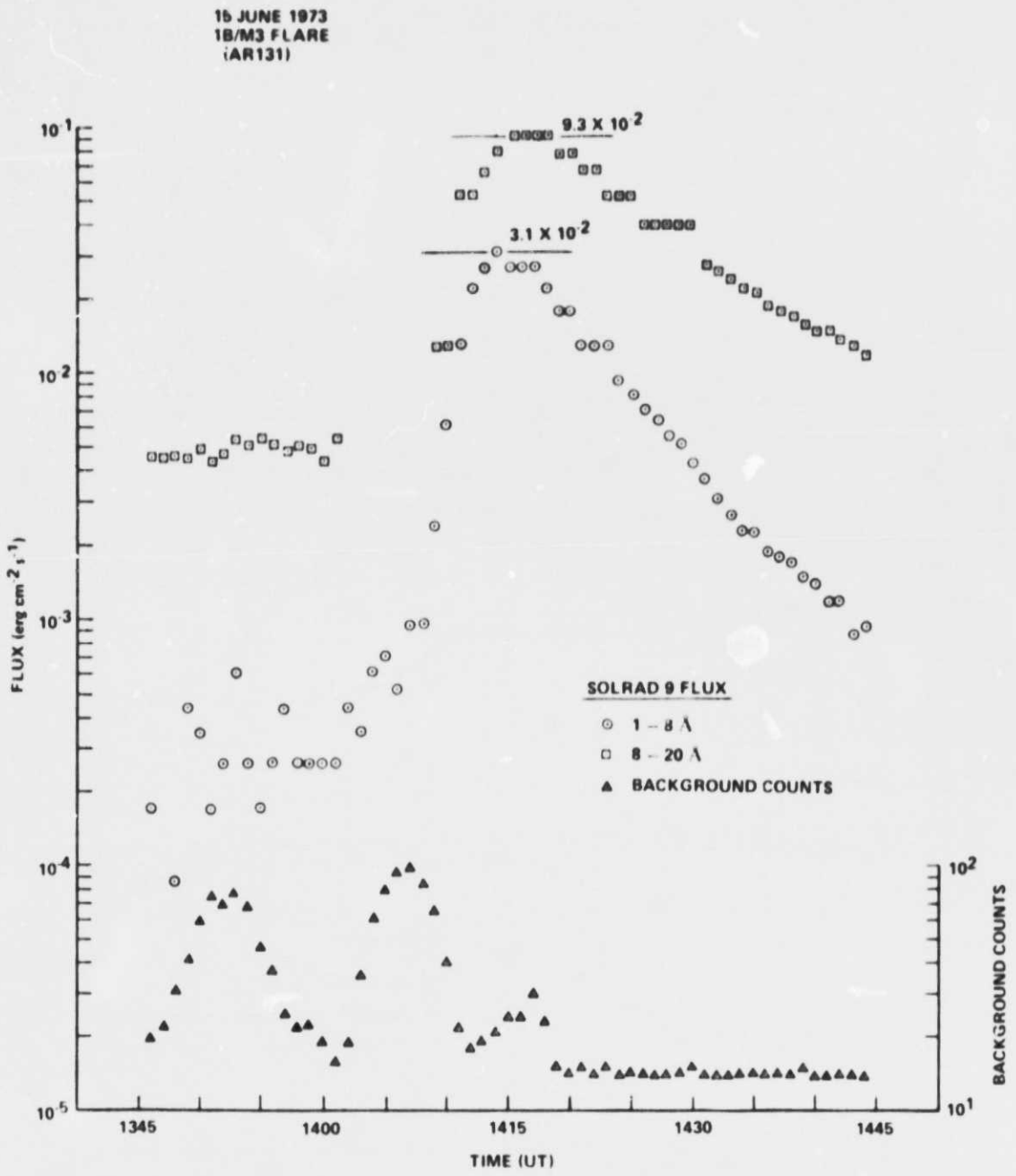

Figure 4. SOLRAD 9 flux (1 to 8 Å, 8 to 20 Å) and background counts for the 15 June 1B/ M3 flare in AR131 (1346 to 1444 UT).

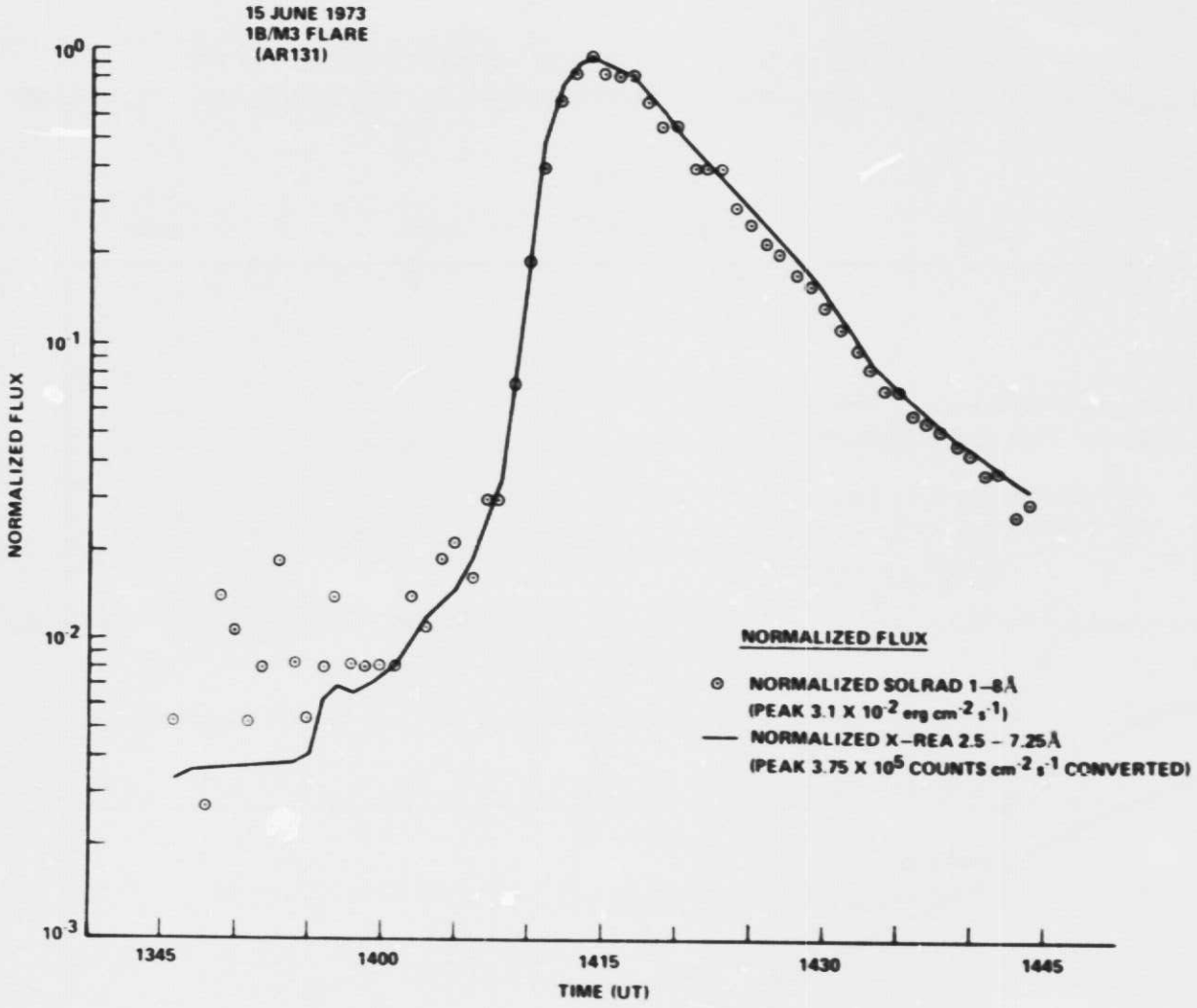

Figure 5. Normalized flux (X-REA beryllium counter total and SOLRAD 9 1 to 8 Å) for the 15 June 1973 1B/ M3 fiare in AR131 (1346 to 1444 UT).

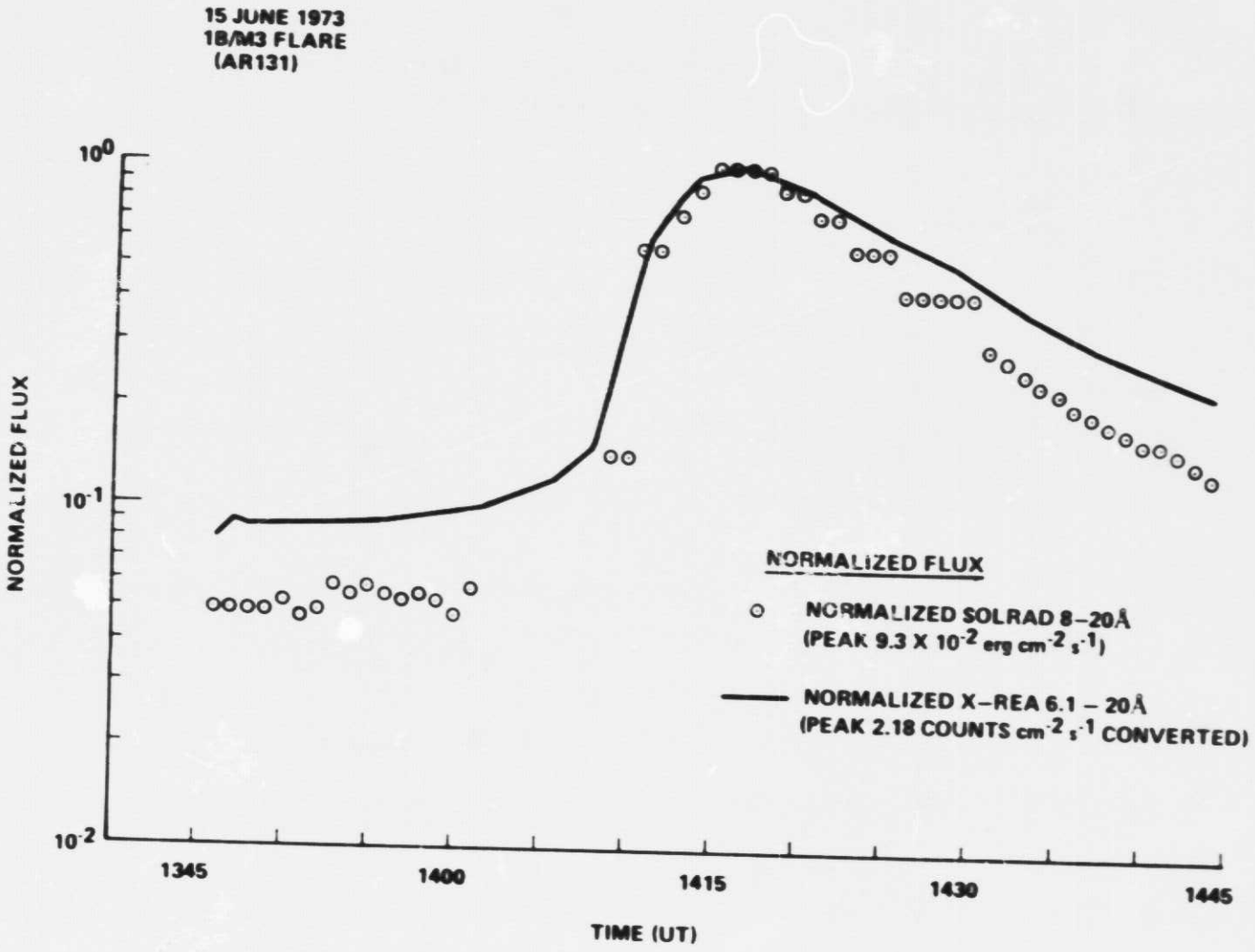

Figure 6. Normalized flux (X-REA aluminum counters total and SOLRAD 9 8 to 20 Å) for the 15 June 1973 1B/ M3 flare in AR131 (1346 to 1444 UT).

in the X-REA aluminum counter and, perhaps, to slightly different bandpasses. It is concluded that the X-REA aluminum counter did observe real changes in the solar x-ray emission; however, the analysis of its data is hampered by noise.

Regarding the comparison of the X-REA and SOLRAD counters it is also noted that the smoothness of the X-REA data and the ability of the counters to record subtle changes in the x-ray emission may be indications that the X-REA counters were, indeed, the more sensitive of the two instruments. Hence, the X-REA counter, with its 2.5 s time resolution, may be of considerable benefit for describing rapid intensity variations in solar x-ray emissions needed for correlations with radio burst data and the like.

To ascertain the absolute calibration of the X-REA, one of two different approaches can be followed. First, it can be assumed that the counters behaved as theoretically predicted; therefore, by correcting for counter efficiencies, adjusting for bandpasses, and multiplying the resultant numbers by appropriate mean photon energies (e.g., assume that all the counts can be described by using the midwavelength energy values in a conversion from counts $cm^{-2}\ s^{-1}$ to erg $cm^{-2}\ s^{-1}$), one can deduce fluxes in terms of erg $cm^{-2}\ s^{-1}$, which should be comparable to SOLRAD 9 fluxes. A second approach assumes that at least two energy channels in one of the counters (e.g., channels 5 and 6 in the beryllium counter) are accurate. One uses these energy channels and the model spectrum to deduce a temperature for the peak of the event. Then, by working backwards, one can deduce the necessary counts $cm^{-2}\ s^{-1}$ to give such a temperature in ratios between the assumed true energy channels and the suspect channels (or totals). In this way one can determine the authenticity of each channel (and total) relative to the assumed true energy channels and, by the first method outlined previously, compare the results with SOLRAD 9.

Following the first method, the beryllium counter data are a factor of 3.85 lower than the corresponding SOLRAD 9 1 to 8 Å values for the period 1406 to 1444 UT. This discrepancy may be attributed to a combination of factors: the correctness of the SOLRAD 9 1 to 8 Å values, the accuracy of the X-REA efficiency determinations, the exactness of the bandwidth adjustment (approximated by the expression $\Delta\lambda$ X-REA/$\Delta\lambda$ SOLRAD 9, where $\Delta\lambda$ is simply the instrument bandpass; for the beryllium counter, the adjusting factor is 0.68), and the preciseness of using the mean photon energy calculated from the mean wavelength of the beryllium counter (equal to 4.06×10^{-9} erg/count, assuming $\bar{\lambda} = 4.88$ Å) to be representative of the entire spectrum. A similar result is observed for the aluminum counter data for the period 1346 to 1401 UT,

when a factor of 1.66 lower than the corresponding SOLRAD 9 8 ', 20 Å values is noted. However, this factor changes greatly with time, being 0.81 higher for the period 1410 to 1420 UT, 0.40 for the period 1421 to 1430 UT, and 0.18 for the period 1431 to 1444 UT. These discrepancies, in addition to those factors already described, may be attributed to noise in the aluminum counter, which apparently is count-rate dependent.

From EUV spectral line data, Cheng[3] has deduced a peak temperature of 14×10^6 K. This value is virtually identical to one deduced using the ratio beryllium channel 6 to beryllium channel 5, which yields a peak temperature of 14.5×10^6 K. Thus, by assuming these channels to be correct, one can take additional ratios, in particular beryllium channels 5 + 6 to beryllium total, beryllium channels 5 + 6 to aluminum total, beryllium total to aluminum total, and beryllium 5 + 6 to aluminum 3 + 4, to deduce their corresponding fluxes and compare these fluxes with the observed fluxes to determine any instrumental effects. Unfortunately, this approach has only one reference point, i.e. the peak temperature, and, as such, can really only be applied to the peak temperature time. If one assumes that the beryllium channels 5 and 6 are accurate over the entire event interval, then one can determine the accuracies of the total counts for the same overall period.

Figure 7 displays the observed beryllium channel 6 to channel 5 ratio as a function of time and its associated temperature profile. One observes preflare ratios to be approximately 0.45, indicative of temperatures of approximately 4.5×10^6 K. The ratio (hence, temperature) and the flux (Fig. 2, beryllium channels 5 and 6) show increased values beginning about 1355 UT, peaking approximately 1411 to 1412 UT in temperature (14.5×10^6 K) and 1413 to 1414 UT in flux. Thereafter, the values decrease slowly with the exception of a slight temperature enhancement at approximately 1426 UT. A data dropout is noted at 1430 UT. This temperature profile is taken as baseline for comparisons with the aforementioned ratios (observed values and calculated values based on the beryllium channels 6 to 5 reference).

Figure 8 is the result of this intercomparison between the baseline reference channels beryllium 5 + 6 and the beryllium counter total. Plotted are the observed ratio, observed temperature (based on the observed ratio), and the calculated ratio, computed by assuming the beryllium channel 6/5 temperature profile (also plotted) to be correct and determining what the ratio must be to give such a temperature. One notices that the shape of the curves for the observed and calculated ratios are similar, indicating that the beryllium counter

3. Private communication with C. C. Cheng.

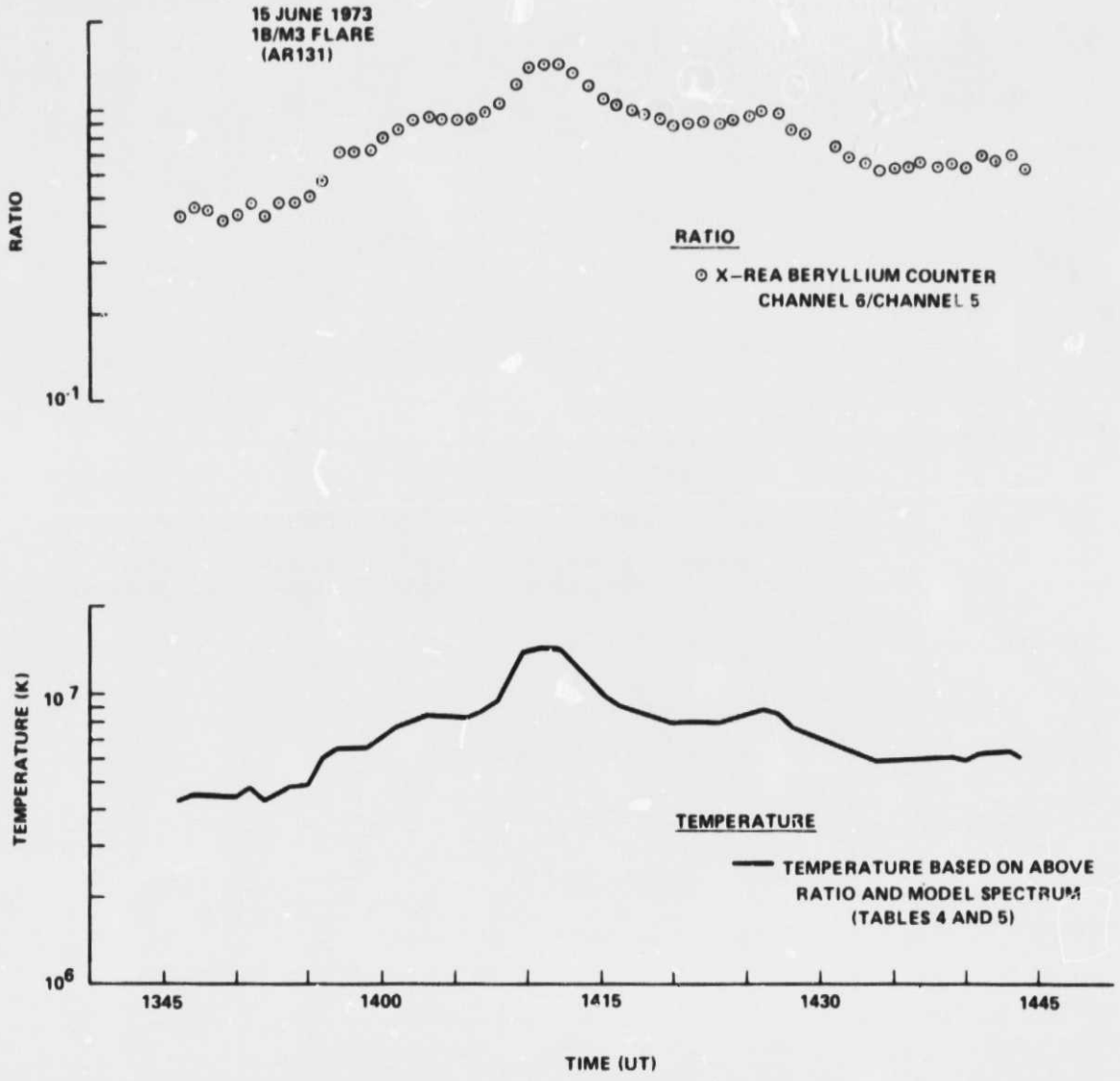

Figure 7. X-REA channel ratio profile (beryllium counter channel 6 to channel 5) and its associated temperature profile for the 15 June 1973 1B/ M3 flare in AR131 (1346 to 1444 UT).

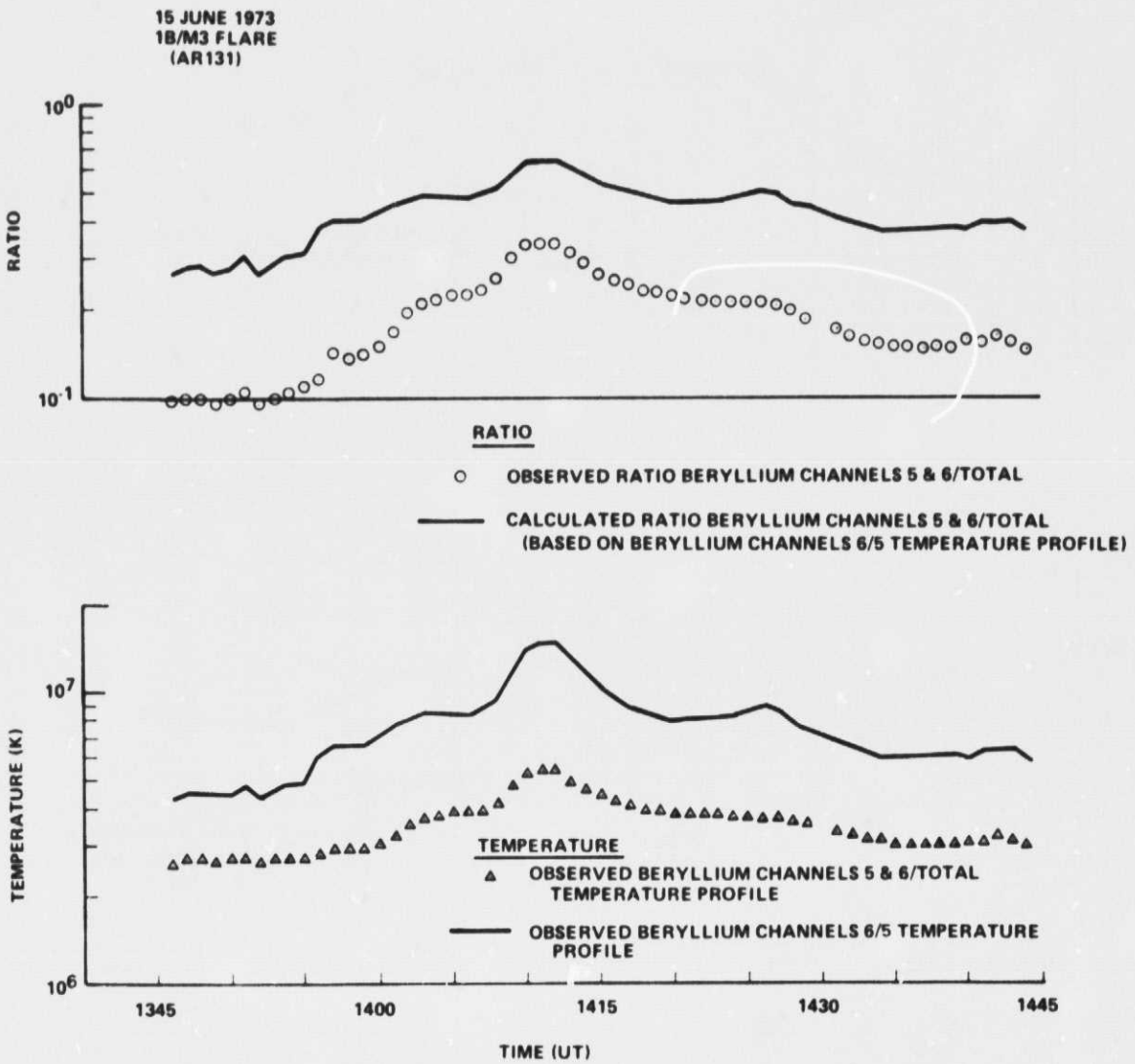

Figure 8. Comparison of observed X-REA channel ratio profile (beryllium counter channels 5 + 6 total) and calculated profile; comparison of observed temperature profiles.

remained fairly stable and did not introduce an appreciable number of noise counts. However, as evidenced in Figure 9, the aluminum counter showed a great deal of variation during the event. Figure 10 illustrates the time-profile variation of the two counters more clearly. First, one notes that the total observed counts in both counters are below the calculated values using the beryllium channels 6/5 ratio and their sum. This may be attributed partly to degradated counters. Second, the beryllium counter, as noted earlier, appears to have been fairly stable during the event. Some variation is however, observed during the rise portion of the flare, but the effect is quite small, especially in comparison to that of the aluminum counter. An average multiplier value of approximately 2.41 is obtained. Third, no one average multiplier value truly represents the aluminum counter time-profile variation. One observes that the aluminum counter appeared to improve (i.e., have a lower multiplier value) as the event progressed, especially between 1410 and 1444 UT. During this interval its average multiplier value is approximately 3.72. The average value for the preflare portion (i.e., 1346 to 1353 UT) is 7.10 and for the flare-rise portion (i.e., 1354 to 1409 UT) is 13.1. A weighted average for these three time intervals yields an average multiplier value of approximately 6.77. Because of this variation, it is concluded that ratios involving the aluminum counter total counts are unreliable.

To ascertain whether or not the variation in the aluminum counter total counts extends to all aluminum counter channels, one can take ratios of selected aluminum counter channels with the beryllium channels 5 + 6. Because the ratio of beryllium channels 5 + 6 to aluminum channels 3 + 4 is theoretically a good indicator of temperature (Table 5), it will be used here. Figure 11 depicts the observed beryllium channels 5 + 6 to aluminum channels 3 + 4 ratio profile as well as its observed temperature profile. The beryllium channels 6/5 reference temperature profile is also plotted. The two temperature profiles are quite similar, and their spread is always less than 2.4×10^6 K. While the reference ratio determines an average peak temperature of 14.5×10^6 K, the beryllium channels 5 + 6 to aluminum channels 3 + 4 ratio yields a temperature of 15.9×10^6 K. The aluminum counter channels 3 + 4 variation is only slightly apparent in the temperature profile between the two intervals 1412 to 1426 UT and 1426 to 1444 UT, suggesting that the variation in the aluminum counter total counts may be attributed chiefly to the lower energy channels.

Completing the second method to directly compare the X-REA and SOLRAD 9 data on the same energy scale, the previous results have been compared with the results of the first method. The beryllium counter data are

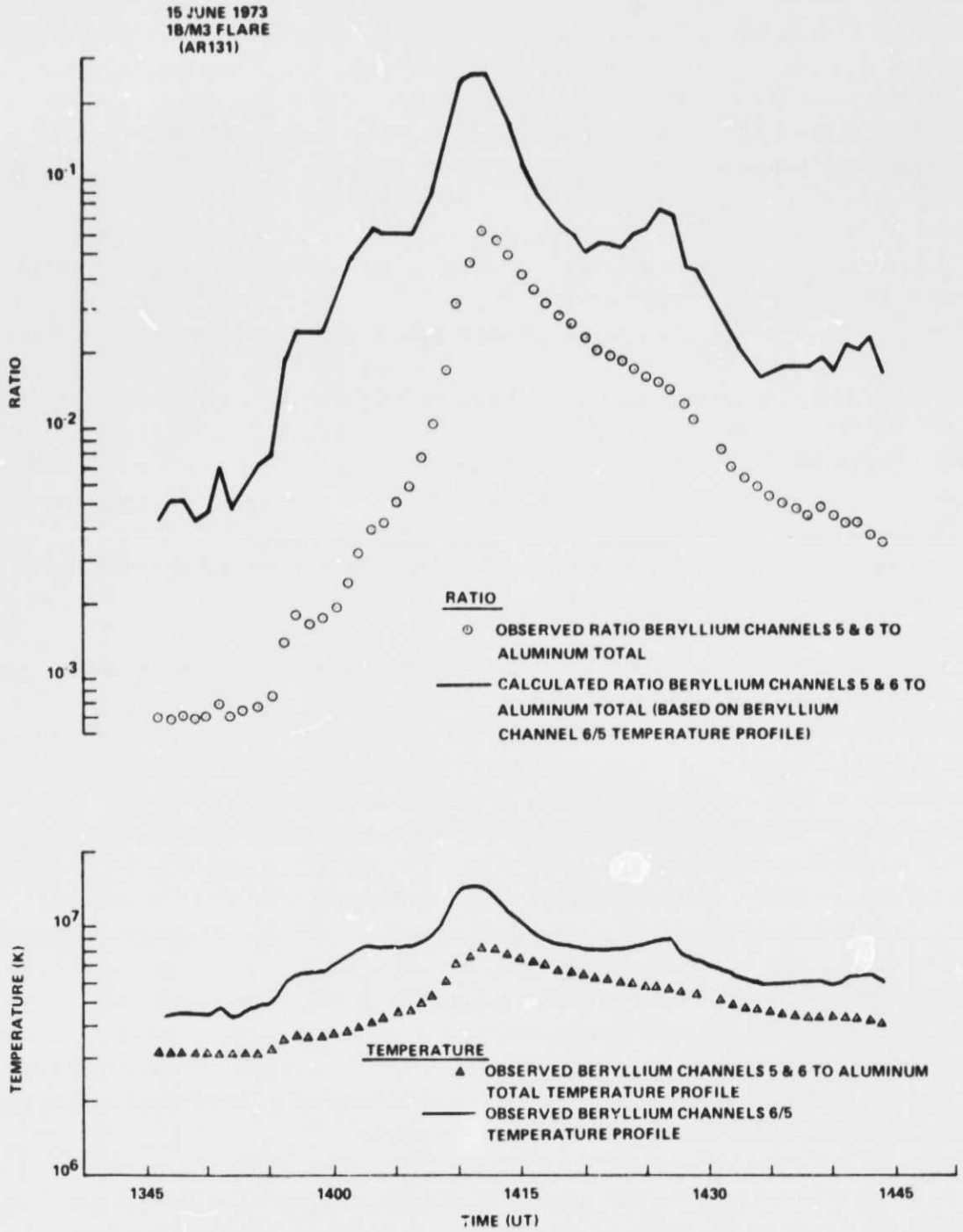

Figure 9. Comparison of observed X-REA channel ratio profile (beryllium counter channels 5 + 6 to aluminum counter total) and calculated profile; comparison of observed temperature profiles.

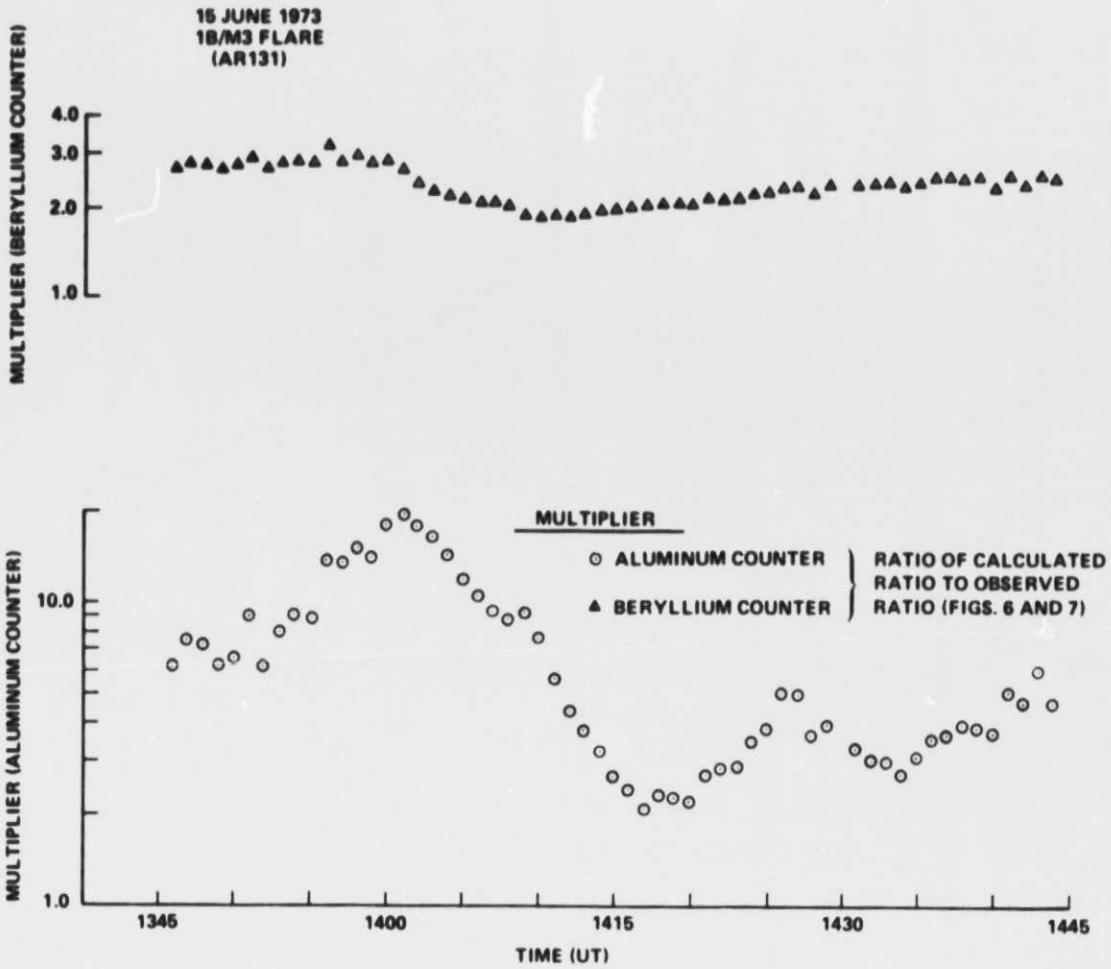

Figure 10. Time-profile variations (multiplier versus time).

found to be still low by a factor of approximately 1.6 in comparison to the SOLRAD 9 1 to 8 Å data. This suggests that at least part of the discrepancy may be attributed to an inappropriate mean photon energy conversion factor. Thus, instead of the value 4.06×10^{-9} erg/count for $\overline{\lambda} = 4.88$ Å, one should use the value 6.5×10^{-9} erg/count, implying a $\overline{\lambda} = 3.05$ Å. The variation in the aluminum counter data, attributed to noise, makes such an intercomparison somewhat cumbersome. Hence, no attempt has been made to complete the second method for the aluminum counter data.

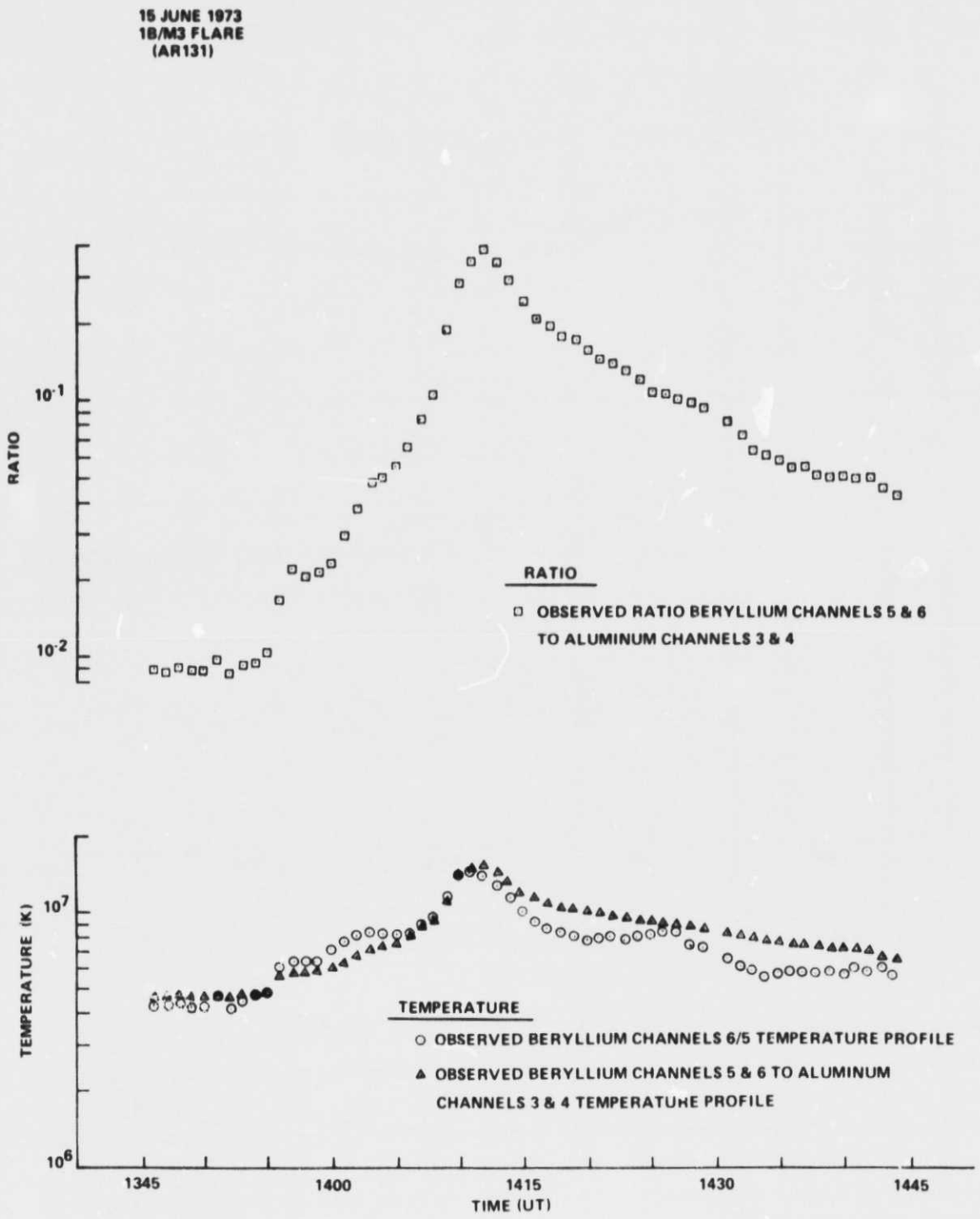

Figure 11. Observed X-REA channel ratio profile (beryllium counter channels 5 + 6 to aluminum counter channels 3 + 4) and comparison of observed temperature profiles (beryllium counter channels 5 + 6 to aluminum counter channels 3 + 4, and beryllium counter channels 6 to 5) for 15 June 1973 1B/ M3 flare in AR131 (1346 to 1444 UT).

The analysis of the X-REA data concerning the determination of the physical parameters of the event is summarized as follows. The beryllium counter channels 6/5 ratio yields an average peak temperature of 14.5×10^6 K at 1411 to 1412 UT. The beryllium channels 5 + 6 to aluminum channels 3 + 4 ratio yields an average peak temperature of 15.9×10^6 K at 1412 UT. Thus, a mean average peak temperature of 15.2×10^6 K at 1412 UT is deduced. Using these two ratios and their associated temperature profiles, one can deduce average emission measure values. Based on the beryllium channels 6/5 ratio and its associated temperature profile, a value of 9.51×10^{48} cm^{-3} is found for the average peak emission measure occurring at 1417 UT. This is to be compared with the value of 5.08×10^{48} cm^{-3} at 1416 UT deduced from the beryllium channels 5 + 6 to aluminum channels 3 + 4 ratio and its associated temperature profile. Thus, a mean average peak emission measure of 7.24×10^{48} cm^{-3} at 1416 UT is determined, which corresponds to a mean average electron density of 2.66×10^{10} cm^{-3}, assuming a volume of 10^{28} cm^3. Figure 12 depicts the mean average values of temperature, emission measure, and electron density (assuming a volume 10^{28} cm^3) as a function of time for the event.

V. DISCUSSION

The analysis of the 15 June 1973 event is important for several reasons. First, it was the major flare of the first Skylab mission and, in fact, one of the largest flares observed over the entire Skylab operational period. Second, since a number of instruments observed it, this flare may be used as a reference or calibration event. A large number of papers [25-54] already have been published concerning the flare. Although it is beyond the scope of this report to summarize all the results concerning the 15 June 1973 event, an attempt is made to highlight some of the findings as related to temperature, density, and flux variation with time.

Results of the analysis of the X-REA data indicate that the x-ray emission showed signs of becoming enhanced as early as 1355 UT, peaking in the 2.5 to 7.25 Å band at 1414 UT and in the 6.1 to 20 Å band at 1416 to 1417 UT, and then slowly decaying, reaching a value of 3.5×10^{-2} times the peak normalized flux in the 2.5 to 7.25 Å band at 1444 UT. An increase in temperature and a decrease in density are concurrent with the initial flux increase. Temperature and density show slow increases between 1401 and 1408 UT and rapid increases

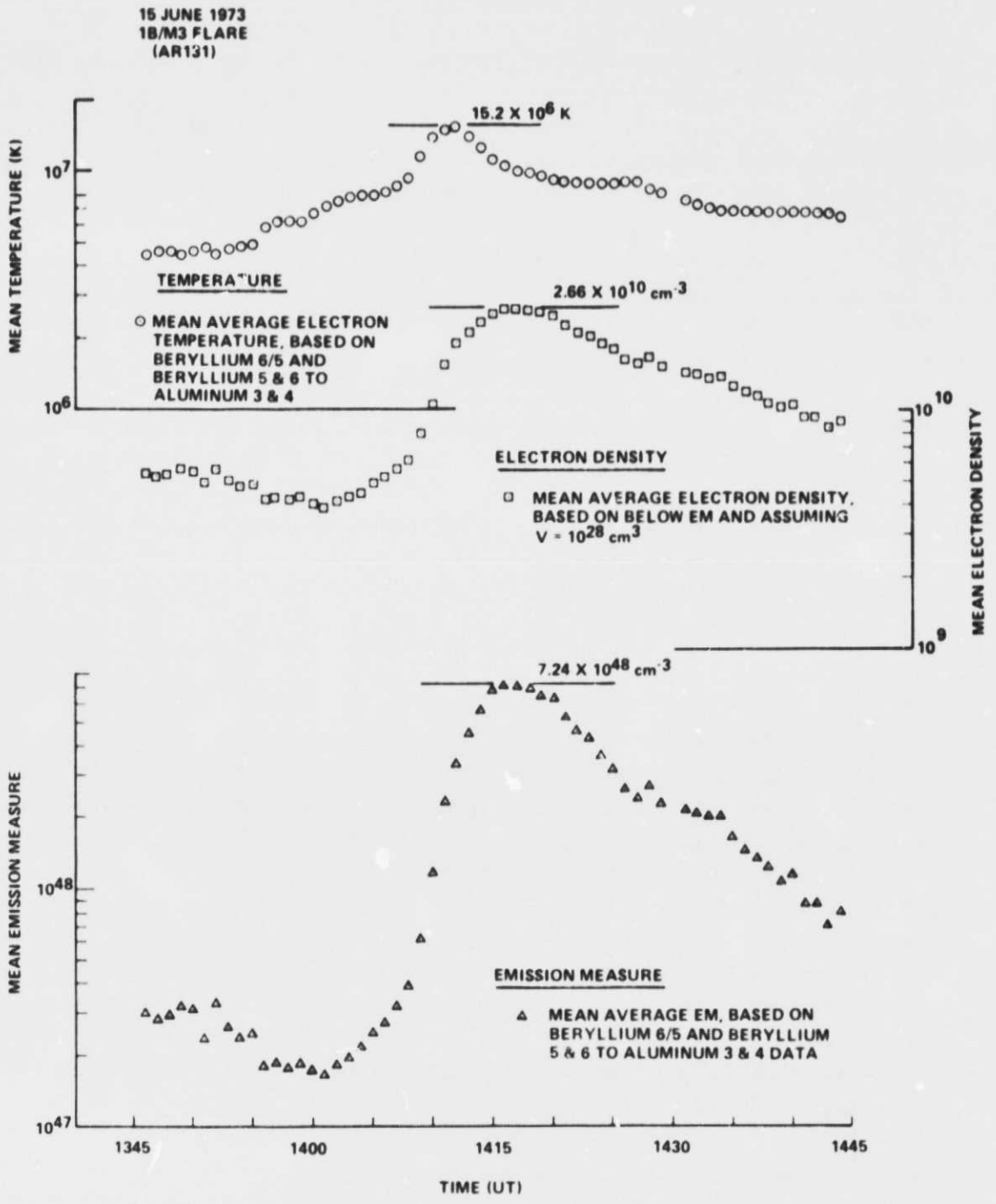

Figure 12. Summary of physical parameter determination results for the 15 June 1973 1B/ M3 flare in AR131 (1346 to 1444 UT), based on averaging values deduced from ratios of beryllium counter channels 6 to 5 and beryllium counter channels 5 + 6 to aluminum counter channels 3 + 4.

after 1408 UT. The temperature peaks at 1412 UT, having a value of approximately 15.2×10^6 K (approximately ±20 percent), and the density peaks at 1416 to 1417 UT, having a value of approximately 2.66×10^{10} cm^{-3} (assuming a flare plasma volume of 10^{27} cm^3). Temperature and density decrease after their respective maxima, with some indication of continued heating occurring between 1420 and 1427 UT and a corresponding lessening of the density decay slope between 1427 and 1434 UT. The x-ray manifestation of the flare further indicates that it took, assuming the x-ray enhancement start at 1355 UT, approximately 16 min to attain 0.5 times the peak flux value from background, only 3 min to reach peak from the 0.5 times the peak flux value, and 7 min to decay from peak to 0.5 times the peak flux value.

A comparison of the X-REA results with some of the results reported in the literature shows good agreement. In particular, Widing and Cheng [25] report a peak temperature of 16×10^6 K, and more recently Cheng reports a peak temperature of 14×10^6 K. The X-REA peak temperature lies between these values and certainly, with its 20 percent error bars, encompasses them. Widing and Cheng [25] also suggest that the temperature dropped below 10×10^6 K at 1419 UT, a suggestion confirmed by the X-REA results. They also report that the electron density was 5×10^{10} cm^{-3} (assuming a flare volume of 10^{27} cm^3) at 1412 UT, which is also confirmed by X-REA results (assuming a volume of 10^{27} cm^3 implies a density of 4.9×10^{10} cm^{-3} at 1412 UT). The X-REA data, however, cannot confirm the suggestion that the temperature had dropped to 5×10^6 K at 1423 UT. This perhaps can be explained by the large field-of-view of the X-REA in comparison to a small slit used in the Naval Research Laboratory instrument. At no time were temperatures found to exceed approximately 17×10^6 K, observed in the 2.5 s resolution data. (It must be recalled that the temperatures and densities presented previously are based on 1 min averages of the X-REA data. Slightly higher and lower values surrounding this mean are noted when using the 2.5 s resolution data.) This may be somewhat contradictory to the view presented by Brueckner [35], who explains the flare in terms of a hot kernel at a temperature greater than 20×10^6 K surrounded by a hot cloud at 20×10^6 K. The results are, however, in agreement with those of Sandlin et al. [53], who suggest a peak temperature less than 20×10^6 K.

REFERENCES

1. Hoover, R. B., Thomas, R. J., and Underwood, J. H.: Advances in Solar and Cosmic X-Ray Astronomy: A Survey of Experimental Techniques and Observational Results. Advances in Space Science and Technology (ed., F. I. Ordway, III), vol. 11, Academic Press, Inc., New York, New York, 1972, pp. 1-214.

2. Horan, D. M.: Electron Temperature and Emission Measure Variation During Solar X-Ray Flares. Sol. Phys. 21, 1971, pp. 188-197.

3. Dere, K. P., Horan, D. M., and Kreplin, R. W.: A Multithermal Analysis of Solar X-Ray Emission. Sol. Phys. 36, 1974, pp. 459-472.

4. Vaiana, G. S., Krieger, A. S., and Timothy, A. F.: Identification and Analysis of Structures in the Corona from X-Ray Photography. Sol. Phys. 32, 1973, pp. 81-116.

5. Walker, A. B. C. Jr., Mayfield, E. B., McKenzie, D. L., and Underwood, J. H.: The Temperature Structure of a Coronal Active Region. B.A.A.S. 6, 1974, pp. 296-297.

6. Vorpahl, J. A., Tandberg-Hanssen, E., and Smith, J. B. Jr.: Coronal Plasma Parameters in a Long Duration X-Ray Event Observed by Skylab. The Aerospace Corporation (Preprint), Astrophys. J. (accepted), 1976.

7. Smith, J. B. Jr., Underwood, J. H., McKenzie, D. L., and Reichmann, E. J.: Analysis of Selected Solar Features from X-Ray Filtergrams. B.A.A.S. 8, 1976, p. 317.

8. Smith, J. B. Jr., Speich, D. M., Wilson, R. M., Tandberg-Hanssen, E., and Wu, S. T.: Prominence Mass Ejections and Their Effects on the Corona. I. The Eruptive Prominence of 21 August 1973 and the Surge of 4 December 1973. Sol. Phys. (submitted), 1976.

9. Walsh, E. J., Sokolowski, T. I., Miller, G. M., Cofield, K. L. Jr., Douglas, J. D., Lewter, B. J., Burke, H. O., and Davis, A. J.: Design Characteristics of a Skylab Soft X-Ray Telescope. Proc. S.P.I.E. 44, 1974, pp. 175-184.

REFERENCES (Continued)

10. Underwood, J. H., Milligan, J. E., deLoach A. C., and Hoover, R. B.: The S-056 X-Ray Telescope Experiment on the Skylab-Apollo Telescope Mount. Appl. Opts. (accepted), 1976.

11. deLoach, A. C., Hoover, R. B., Wilson, R. M. Milligan, J. E., and Underwood, J. H.: The Skylab ATM/S-056 Solar X-Ray Telescope: Design and Performance. To be submitted as NASA TN D, 1976.

12. Bliven, W., Foreman, J. W. Jr., and Walsh, E. J.: Space Sensors for X-Ray Astronomy. Sperry Rand Eng. Rev. 22, 1969, pp. 31-37.

13. Walker, A. B. C. Jr.: The Coronal X-Spectrum: Problems and Prospects. Space Sci. Rev. 13, 1972, pp. 672-730.

14. Walker, A. B. C. Jr.: Interpretation of the X-Ray Spectra of Solar Active Regions. Solar Gamma-, X-, and EUV Radiation (ed., S. P. Kane), IAU Symp. no. 68, D. Reidel Publ. Co., Dordrecht, Holland, 1975, pp. 73-100.

15. Doschek, G. A.: The Solar Flare Plasma: Observation and Interpretation. Space Sci. Rev. 13, 1972, pp. 765-821.

16. Doschek, G. A : X-Ray and EUV Spectra of Solar Flares and Laboratory Plasma. Solar Gamma-, X-, and EUV Radiation (ed., S. P. Kane), IAU Symp. no. 68, D. Reidel Publ. Co., Dordrecht, Holland, 1975, pp. 165-181.

17. Kahler, S.: Thermal and Nonthermal Interpretations of Flare X-Ray Bursts. Solar Gamma-, X-, and EUV Radiation (ed., S. P. Kane), IAU Symp. no. 68, D. Reidel Publ. Co., Dordrecht, Holland, 1975, pp. 211-231.

18. Brown, J. C.: On the Thermal Interpretation of Hard X-Ray Bursts from Solar Flares. Coronal Disturbances (ed. G. Newkirk, Jr.), IAU Symp. no. 57, D. Reidel Publ. Co., Dordrecht, Holland, 1974, pp. 395-412.

REFERENCES (Continued)

19. Brown, J. C.: The Interpretation of Hard and Soft X-Rays from Solar Flares. Phil. Trans. Roy. Soc. London (Series A), 281, 1976, pp. 473-490.

20. DeJager, C., Kuperus, M., and Rosenberg, H.: Solar Flares. Phil. Trans. Roy. Soc. London (Series A), 281, 1976, pp. 507-513.

21. Peterson, L. E., Datlowe, D. W., and McKenzie, D. L.: Thermal and Nonthermal X-Ray Bursts Observed from OSO-7. High Energy Phenomena on the Sun (eds., R. Ramaty and R. G. Stone), NASA SP-342, NASA, Washington, D. C., 1973, pp. 132-146.

22. Doschek, G. A. and Meekins, J. F.: Soft X-Ray Flare Spectra. High Energy Phenomena on the Sun (eds., R. Ramaty and R. G. Stone), NASA SP-342, NASA, Washington, D. C., 1973, pp. 262-275.

23. Hirman, J., Losey, R., and Heckman, G.: A Compilation of Solar Flares Reported During the SKYLAB Mission (1 May 1973-28 February 1974), Preliminary Copy. Space Environment Services Center, Space Environment Laboratory NOAA, Boulder, CO, 1975.

24. Scherrer, V. E. and Sandlin, G. D.: Flare Atlas and Users Instruction Guide for NRL Flare Data 15 June, 5 and 7 September 1973. NRL Instruction Book No. 161, 1976.

25. Widing, K. G. and Cheng, C. -C.: On the Fe XXIV Emission in The Solar Flare of 1973 June 15. Astrophys. J. (Letters), 194, 1974, pp. L111-L113.

26. Spicer, D. S. and Cheng, C. -C.: The Screw Pinch and the Solar Flare. B.A.A.S. 6, 1974, p. 294.

27. Spicer, D. S.: A Restrictive Screw Instability Model of a Solar Flare. B.A.A.S. 7, 1975, p. 397.

28. Kepple, P. C. and Spicer, D. S.: A Time Dependent Study of Conductive Heat Flow in a Flaring Arch. B.A.A.S. 7, 1975, pp. 397-398.

REFERENCES (Continued)

29. Cheng, C. -C. and Widing, K. G.: Energy Release and Thermal Structure in Solar Flares. B.A.A.S. 7, 1975, p. 424.

30. Widing, K. G.: Fe XXIV Emission in Solar Flares Observed with the NRL/ATM XUV Slitless Spectrograph. Solar Gamma-, X-, and EUV Radiation (ed., S. P. Kane), IAU Symp. no. 68, D. Reidel Publ. Co., Dordrecht, Holland, 1975, pp. 153-163.

31. Godoli, G., Sciuto, V., and Zappala, R. A.: Optical Study of June 15, 1973 Flare. Skylab Solar Workshop (ed., G. Righini), Osservazioni e Memorie, Arcetri Astrophysical Observatory, Fascicolo 104, Baccini and Chiappi, Florence, Italy, 1974, pp. 169-174.

32. Godoli, G., Sciuto, V., and Zappala, R. A.: Optical and Magnetic Study of the Active Regions ATM 131 and 137 at the Photospheric and Chromospheric Levels. Skylab Solar Workshop (ed., G. Righini), Osservazioni e Memorie, Arcetri Astrophysical Observatory, Fascicolo 104, Baccini and Chiappi, Florence, Italy, 1974, pp. 192-201.

33. Brueckner, G. E.: Ultraviolet Emission Line Profiles of Flares and Active Regions. Solar Gamma-, X-, and EUV Radiation (ed., S. P. Kane), IAU Symp. no. 68, D. Reidel Publ. Co., Dordrecht, Holland, 1975, pp. 135-151.

34. Brueckner, G. E., Bohlin, J. D., Moe, O. K., Nicolas, K. R., Purrell, J. D., Scherrer, V. E., Sheeley, N. R. Jr., and Tousey, R.: The 1175Å to 1990Å Ultraviolet Spectrum of Solar Flares. B.A.A.S. 6, 1974, p. 285.

35. Brueckner, G. E.: ATM Observations on the XUV Emission from Solar Flares. Phil. Trans. Roy. Soc. London (Ser. A), 281, 1976, pp. 443-459.

36. Brueckner, G. E., Moe, O. K., and Van Hoosier, M. E.: Line Profiles of the Fe XXIV Emission at 192 Å and 255 Å in Solar Flares. B.A.A.S. 7, 1975, p. 357.

REFERENCES (Continued)

37. Doschek, G. A., Feldman, U., Dere, K. P., Sandlin, G. D., Van Hoosier, M. E., Purcell, J. D., and Tousey, R.: Forbidden Lines of Highly Ionized Iron in Solar Flare Spectra. Astrophys. J. (Letters), 196, 1975, pp. L83-L86.

38. Widing, K. G.: Fe XXIII 263 Å and Fe XXIV 255 Å Emission in Solar Flares. Astrophys. J. (Letters), 197, 1975, pp. L33-L35.

39. Cheng, C. -C. and Widing, K. G.: On the XUV Emissions in Solar Flares Observed with the ATM/NRL Spectroheliograph. B.A.A.S. 7, 1975, p. 356.

40. Cheng, C. -C. and Widing, K. G.: Spatial Distribution of XUV Emission in Solar Flares. Astrophys. J. 201, 1975, p. 735-739.

41. Widing, K. G. and Cheng, C. -C.: Evolution of XUV Plasmas in Solar Flares. B.A.A.S. 7, 1975, p. 424.

42. Poletto, G., Krieger, A., Silk, J. K., Timothy, A., and Vaiana, G.: Extrapolation of Photospheric Magnetic Fields into the Corona. B.A.A.S. 6, 1974, pp. 292-293.

43. Poletto, G., Timothy, A. F., Krieger, A. S., and Vaiana, G. S.: Coronal X-Ray Structures and Coronal Magnetic Fields. Skylab Solar Workshop (ed., G. Righini), Osservazioni e Memorie, Arcetri Astrophysical Observatory, Fascicolo 104, Baccini and Chiappi, Florence, Italy, 1974, pp. 175-191.

44. Poletto, G., Vaiana, G. S., Zombeck, M. V., Krieger, A. S., and Timothy, A. F.: A Comparison of Coronal X-Ray Structures of Active Regions with Magnetic Fields Computed from Photospheric Observations. Sol. Phys. 44, 1975, pp. 83-99.

45. Underwood, J. H.: X-Ray Observations of the Flare of June 15, 1973. B.A.A.S. 7, 1975, p. 438.

REFERENCES (Continued)

46. Kahler, S. W. and Buratti, B. J.: Preflare X-Ray Morphology of Active Regions Observed with the AS&E Telescope on Skylab. ASE-3776 (Preprint), 1975.

47. Henze, W., Reichmann, E. J., deLoach, A. C., Hoover, R. B., McGuire, J. P., Tandberg-Hanssen, E., and Wilson, R. M.: Analysis of SKYLAB Soft X-Ray Observations of Solar Active Region 131 (McMath 12379). B.A.A.S. 7, 1975, pp. 443-444.

48. Feldman, U., Brown, C. M., Doschek, G. A., Moore, C. E., and Rosenberg, F. D.: The XUV Spectrum of CI Observed from SKYLAB During a Solar Flare. NRL Preprint, 1975.

49. Vaiana, G. S., Kahler, S., Krieger, A., Pallavicini, R., and Silk, J. K.: An X-Ray Flare from Skylab: Results and Interpretation. B.A.A.S. 6, 1974, p. 265.

50. Pallavicini, R., Kahler, S., Krieger, A. S., Silk, J. K., and Vaiana, G. S.: X-Ray and Radio Emission for the June 15, 1973 Solar Flare. Skylab Solar Workshop (ed., G. Righini), Osservazioni e Memorie, Arcetri Astrophysical Observatory, Fascicolo 104, Baccini and Chiappi, Florence, Italy, 1974, pp. 157-168.

51. Pallavicini, R., Vaiana, G. S., Kahler, S. W., and Krieger, A. S.: Spatial Structure and Temporal Development of a Solar X-Ray Flare Observed from Skylab on June 15, 1973. Sol. Phys. 45, 1975, pp. 411-433.

52. Brueckner, G. E., Patterson, N. P., and Scherrer, V. E.: Spectroscopic Far Ultraviolet Observations of Transition Zone Instabilities and Their Possible Role in a Pre-Flare Energy Build-Up. NRL Preprint, 1976,

53. Sandlin, G. D., Brueckner, G. E., Scherrer, V. E., and Tousey, R.: High Temperature Flare Lines in the Solar Spectrum 171 Å - 630 Å. Astrophys. J. (Letters), 205, 1976, pp. L47-L50.

REFERENCES (Concluded)

54. Henze, W. Jr., Krall, K. R., Reichmann, E. J., Smith, J. B. Jr., and Wilson, R. M.: Physical Properties and Energy Analysis of the 15 June, 1973 Flare Based on Skylab Operations. B.A.A.S. 8, 1976, p. 375.

APPROVAL

THE SKYLAB ATM/S-056 X-RAY EVENT ANALYZER: INSTRUMENT DESCRIPTION, PARAMETER DETERMINATION, AND ANALYSIS EXAMPLE (15 JUNE 1973 1B/M3 FLARE)

By Robert M. Wilson

The information in this report has been reviewed for security classification. Review of any information concerning Department of Defense or Atomic Energy Commission programs has been made by the MSFC Security Classification Officer. This report, in its entirety, has been determined to be unclassified.

This document has also been reviewed and approved for technical accuracy.

Anthony C. deLoach

ANTHONY C. deLOACH
Chief, Solar Sciences Branch

William C. Snoddy

WILLIAM C. SNODDY
Chief, Astronomy and Solid State Physics Division

Charles A. Lundquist

CHARLES A. LUNDQUIST
Director, Space Sciences Laboratory

☆ U.S. GOVERNMENT PRINTING OFFICE 1976—641-255/572 REGION NO. 4